SoilNutri: A Passive Metasurface-based, Low-cost System for Soil Moisture and Nitrogen Monitoring

JUEXING WANG, Michigan State University, United States
BINBIN XIE, University of Texas at Arlington, United States
YIMENG LIU, Michigan State University, United States
MINHAO CUI, Seoul National University, Republic of Korea
XIAO ZHANG, University of Michigan-Dearborn, United States
GUANGJING WANG, University of South Florida, United States
KE SUN, University of Michigan, Ann Arbor, United States
ZHICHAO CAO, Michigan State University, United States
HUACHENG ZENG, Michigan State University, United States
QINGXU JIN, Michigan State University, United States
YOUNSUK DONG, Michigan State University, United States
HUI LI, Michigan State University, United States
JIE XIONG, Nanyang Technological University, Singapore
TIANXING LI*, Michigan State University, United States

Smart agriculture requires efficient and scalable sensing of key soil parameters. While recent wireless sensing systems provide low-cost alternatives, active designs depend on powered underground components with potential instability and contamination risks, whereas passive battery-free approaches suffer from limited accuracy and are typically restricted to moisture detection. This work presents SoilNutri, a fully passive and battery-free metasurface capsule that enables simultaneous, high-precision monitoring of soil moisture and nitrogen concentration. The system employs a complementary split-ring (CSR) metasurface integrated within a sandwich-structured capsule that provides electromagnetic isolation and stable coupling with the surrounding soil. A lightweight two-stage soil-meta-VAE framework reconstructs soil-distorted reflection spectra and jointly predicts moisture and nitrogen from a shared latent representation. Extensive in-lab and field experiments demonstrate high-precision moisture estimation with 0.64% MAE and ppm-level nitrogen prediction with 5.14 ppm MAE across diverse soil types, depths, and seasonal conditions. With a per-unit cost below $1 and a reusable encapsulated

*Corresponding author.

Authors' Contact Information: Juexing Wang, Michigan State University, United States, wangjuex@msu.edu; Binbin Xie, University of Texas at Arlington, United States, binbin.xie@uta.edu; Yimeng Liu, Michigan State University, United States, liuyime2@msu.edu; Minhao Cui, Seoul National University, Republic of Korea, minhaocui@snu.ac.kr; Xiao Zhang, University of Michigan-Dearborn, United States, zhanxiao@umich.edu; Guangjing Wang, University of South Florida, United States, guangjingwang@usf.edu; Ke Sun, University of Michigan, Ann Arbor, United States, kesuniot@umich.edu; Zhichao Cao, Michigan State University, United States, caozcthu@gmail.com; Huacheng Zeng, Michigan State University, United States, hzeng@msu.edu; Qingxu Jin, Michigan State University, United States, billjin@msu.edu; Younsuk Dong, Michigan State University, United States, dongyoun@msu.edu; Hui Li, Michigan State University, United States, lihui@msu.edu; Jie Xiong, Nanyang Technological University, Singapore, jie.xiong@ntu.edu.sg; Tianxing Li, Michigan State University, United States, litianx2@msu.edu.

ACM 2474-9567/2026/3-ART19
https://doi.org/10.1145/3789674

design, SoilNutri offers a scalable, sustainable, and physically interpretable solution for multi-nutrient, in-situ soil monitoring for next-generation smart agriculture.

CCS Concepts: • **Human-centered computing → Ubiquitous and mobile computing systems and tools**.

Additional Key Words and Phrases: Smart agriculture; Soil sensing; Multi-task learning; Low-cost sensing; Passive metasurface

ACM Reference Format:
Juexing Wang, Binbin Xie, Yimeng Liu, Minhao Cui, Xiao Zhang, Guangjing Wang, Ke Sun, Zhichao Cao, Huacheng Zeng, Qingxu Jin, Younsuk Dong, Hui Li, Jie Xiong, and Tianxing Li. 2026. SoilNutri: A Passive Metasurface-based, Low-cost System for Soil Moisture and Nitrogen Monitoring. *Proc. ACM Interact. Mob. Wearable Ubiquitous Technol.* 10, 1, Article 19 (March 2026), 28 pages. https://doi.org/10.1145/3789674

1 INTRODUCTION

Soil serves as the foundation of agricultural productivity, and the emergence of smart agriculture offers a transformative pathway to enhance crop yield and resource efficiency [5, 27]. By enabling real-time monitoring of key soil parameters, such as moisture content and nutrient availability (e.g., nitrogen concentration), smart systems empower data-driven precision management. Maintaining proper soil moisture supports plant growth while minimizing freshwater consumption [28, 30, 33], and regulating nitrogen levels prevents groundwater contamination and nitrate toxicity [45, 47]. Hence, accurate soil sensing is not only vital for agricultural productivity but also for environmental sustainability and public health protection.

In recent years, wireless sensing systems have played a pivotal role in advancing smart agriculture by providing portable and low-cost solutions for in-situ soil condition monitoring. Tab. 1 presents a detailed comparison of representative wireless soil sensing systems, outlining their signal modalities, sensing range, power requirements, sensing targets, deployment cost, additional setup needs, and overall performance. These systems employ diverse signal modalities, including Wi-Fi [14, 20], LoRa [10, 38, 44], LTE [16], mmWave [12], RFID [43], and optical signals [44]. By analyzing received signal features such as amplitude, phase, or attenuation, these systems can infer fundamental properties such as moisture level.

However, existing wireless soil sensing systems still face two fundamental limitations that hinder their practicality for large-scale farmland deployment. First, systems that rely on active underground sensing units require a continuous power supply for signal generation and data transmission [10, 14, 16, 24, 29, 38, 44]. Although several designs have demonstrated multi-nutrient sensing capabilities with extended battery lifetime, their inherent dependence on onboard power severely limits scalability, long-term operation, and maintenance-free deployment. These limitations motivate the need for a fully battery-free underground sensing architecture, enabling sensing longevity and scalable deployment without being constrained by onboard power availability. Second, passive sensing approaches [12, 15, 20, 22, 43] eliminate the need for underground power by leveraging wireless interrogation signals emitted from surface radars. However, their sensing capability remains largely restricted to soil moisture detection with limited sensitivity, making it difficult to capture weaker but equally critical soil parameters such as nitrogen concentration, which directly affects crop yield and contributes to groundwater contamination.

While existing active sensors require an external power supply and passive sensors are limited to moisture detection, this raises a key question: *Can we design a compact soil sensing system that supports fully passive underground operation while enabling multi-nutrient soil monitoring in a cost-effective manner?*

To address this challenge, we present SoilNutri, a novel passive metasurface-based soil sensing system that enables simultaneous moisture and nitrogen detection without any power supply. By precisely engineering the resonant characteristics of the metasurface, SoilNutri achieves high-resolution soil moisture estimation with a mean absolute error (MAE) of only 0.64%, and accurately quantifies nitrogen concentration with an MAE of 5.14 ppm (mg/kg). Moreover, SoilNutri maintains stable performance across a wide soil moisture range (10%–60%) and

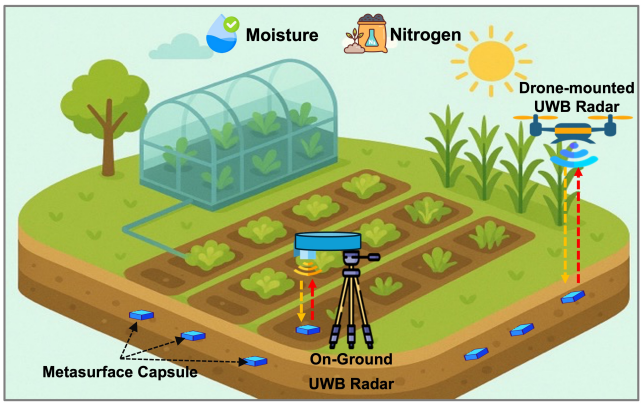

Fig. 1. On-site application scenario of SoilNutri. The metasurface sensing capsule is embedded underground to enable direct interaction with the soil. Variations in soil conditions modulate the spectral characteristics of the reflected signal, which are decoded through signal reconstruction and classification pipelines to jointly infer soil moisture and nitrogen levels with high resolution.

operates robustly under complex underground conditions through a specially designed capsule structure that protects both the top and bottom surfaces of the metasurface. As illustrated in Fig. 1, SoilNutri supports versatile deployment strategies, from ground-based measurements using a tripod to aerial scans via unmanned aerial vehicles (UAVs), providing flexible coverage for both small gardens and large-scale farmland. By combining UAV-assisted mobile data collection with a fully battery-free passive sensing architecture, SoilNutri enables scalable and flexible soil monitoring over large agricultural areas while supporting long-term underground deployment. With a material cost of approximately $1 per buried passive sensor unit and a shared UWB sensing module costing around $150, the system offers a cost-effective and practical pathway toward large-scale, real-world agricultural deployment.

However, several critical challenges remain before realizing this goal. Firstly, the electromagnetic response of a passive metasurface strongly depends on its surface-layer structure and overall permittivity, making it highly susceptible to direct surface-layer contact with the surrounding soil. Previous metasurface designs [12] employed bulky protective tubes to isolate the surface layer and establish a direct propagation path, which is impractical for large-scale farmland deployment. Moreover, in underground environments, the ground layer of the metasurface must fully contact the soil to capture dielectric variations, yet unintended contact with stones or metallic debris can distort the local electromagnetic field and degrade sensing stability. To address these issues, we design a sandwich-structured metasurface capsule that offers both mechanical protection and electromagnetic isolation. It integrates a PETG-based top cover with a thin air layer to prevent surface contamination, and a hydrophilic PTFE membrane at the bottom to maintain stable contact with soil water while blocking unwanted solid interference. By mitigating the interference from both upper and lower interfaces, SoilNutri preserves the underground electromagnetic responses and ensures robust performance across diverse field conditions.

Secondly, even with structural protection, a single metasurface unit can capture only limited permittivity-related information from its spectral response, which is insufficient to infer both soil moisture and nitrogen concentration. In particular, when nitrogen is present at parts-per-million (ppm) levels—approximately four orders of magnitude lower than the concentration of soil moisture—the nitrogen-induced spectral variations are often masked by the dominant moisture effect, making them difficult to isolate. To enhance sensitivity to such subtle changes, we design a complementary split-ring (CSR) configuration that strengthens the coupling between the incident wave and the metasurface structure. This configuration allows fine-tuned control over resonance sharpness,

Table 1. Comprehensive comparison of wireless soil sensing systems.

Method	Signal Type	Sensing Range	Power	Function	Deployment Cost	Extra Setup	Error
Strobe [14]	Wi-Fi	15 cm depth	✔	Moisture	~$100	✗	3%
CoMEt [24]	X310	38 cm depth	✔	Moisture	> $100	✗	1.1%
GreenTag [43]	RFID	2 m	✗	Moisture	$0.05	Tag on Pot	5%
LTE-Soil-Meter [16]	LTE	2.4 km	✔	Moisture	$55	✗	3.15%
Chang et al. [10]	LoRa	100 m	✔	Moisture	$7.5	✗	3.1%
SoilId [15]	UWB	3 m	✗	Moisture	~$5	✗	0.23%
SoilTag [20]	Wi-Fi	13.9 m	✗	Moisture	~$30	✗	2% - 8%
Josephson et al. [22]	UWB	30 cm depth	✗	Moisture	~$5	✗	3.4%
SoilCare [44]	LoRa&VNIR	40 cm depth	✔	Moisture and NPK	~$63.5	Sealing Box	1%
MetaSoil [12]	mmWave	1.5 m	✗	Moisture	$16	Tunnel Inserting	1.2%
SoilNutri (our work)	**UWB**	**40 cm**	✗	**Moisture and Nitrogen**	**$1**	✗	**0.64% and 5.14 ppm**

enabling ppm-scale detection of nitrogen concentration while maintaining signal robustness in moisture-rich conditions. Beyond improving individual sensitivity, we further develop a consolidated metasurface array that integrates two distinct metasurface designs with different geometries and electromagnetic responses. Through the complementary characteristics of these dual resonators, the system achieves richer spectral encoding of soil-related information.

Thirdly, once the passive metasurface has correctly captured the soil-related spectral information, this information must be reliably conveyed through its reflected signals to the aboveground radar receiver. However, underground environments are inherently complex and highly variable across different field conditions and soil types. Even within the same soil category and depth, subsurface heterogeneity can introduce distinct multipath effects, causing spectral distortion and information loss during signal propagation. These distortions hinder the accurate extraction of soil moisture and nitrogen information from the received signal. To address this challenge, we introduce a soil-meta-VAE reconstruction framework that restores the degraded reflection spectrum to its clean, direct-path counterpart, thereby recovering the intrinsic soil information encoded in the amplitude of the frequency spectrum. This reconstruction is guided by the relative spectral coupling between the twin metasurfaces, which provides invariant amplitude references across diverse soil environments. Building on this recovered representation, a shared-latent multi-task network is further developed to jointly predict soil moisture and nitrogen concentration from the reconstructed latent features. By initializing this shared latent space from the pre-trained β-VAE, the network leverages a domain-invariant and physically grounded feature basis, enabling consistent spectral reconstruction and accurate nutrient estimation under varying soil depths and types. Together, this two-stage design achieves robust in-situ sensing by integrating generative reconstruction with physics-guided multi-task prediction.

The total fabrication cost of a consolidated metasurface capsule array is approximately $1, including $0.5 for the two hydrophilic membranes, $0.1 per metasurface array, and $0.3 for the protective top cover and the interconnection between the two distinct metasurfaces. This cost-efficient design enables large-scale field deployment of buried passive sensors at minimal expense. Moreover, the metasurface capsule is reusable under typical field conditions, provided that the protective top enclosure and bottom membrane remain intact without physical damage. While the passive sensing capsules incur only a marginal per-unit cost, the complete system relies on a shared UWB sensing module with a one-time cost of approximately $150, which can be reused across measurements to sequentially query different buried sensors. Together, these characteristics position SoilNutri as a scalable, cost-effective, and infrastructure-light solution for high-resolution in-situ soil monitoring, advancing the vision of ubiquitous and mobile sensing across large agricultural environments.

The main contributions of this work are summarized as follows:

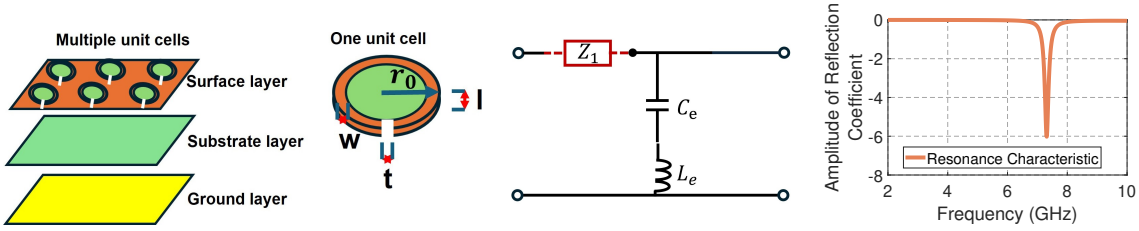

(a) Basic Design (b) Equivalent Circuit (c) Example of Resonance Valley

Fig. 2. Physical structure of metasurface and equivalent circuit of passive metasurface-based sensing.

- We propose SoilNutri, a battery-free passive metasurface-based soil sensing system that enables simultaneous and scalable monitoring of underground soil moisture and nitrogen concentration.
- We introduce a metasurface-enhanced sensing and learning framework that integrates a CSR-based dual-resonator architecture with a soil-meta-VAE inference model to reconstruct underground reflections and support robust joint estimation across varying soil conditions and depths.
- We validate SoilNutri through comprehensive in-lab and field experiments, achieving a mean absolute error of 0.64% in soil moisture estimation and 5.14 ppm in nitrogen sensing, demonstrating its potential for practical agricultural deployment.

2 PRINCIPLE OF PASSIVE METASURFACE-BASED SOIL SENSING

Passive metasurfaces are engineered electromagnetic surfaces designed to enable specific wave–object interactions, and they function as either band-stop filters [9] or band-pass filters [7]. In real-world sensing applications, the band-stop configuration is commonly employed to enable the sensing of a variety of substances, including liquids [11], gases [41], and solid materials [9].

Fig. 2(a) shows the physical composition of the passive metasurface, which consists of three main layers: (1) the surface layer, which hosts the functional metasurface pattern and serves as the main design plane where the resonant structures are implemented; (2) the substrate layer, whose material and thickness are chosen based on the sensing application requirements and fabrication cost considerations; and (3) the ground layer, an optional metallic backing that can enhance the band-stop characteristics by improving signal reflection capability and suppressing internal transmission.

The underlying principle of each unit cell in the passive metasurface can be modeled as an equivalent inductance-capacitance (LC) resonator, as shown in Fig. 2(b), consisting of an effective capacitance C_e and inductance L_e [6, 32]. The inductance is mainly influenced by the geometry of the metallic structure and can be approximated by

$$L_e \approx \mu_0 r_0 \left[\ln\left(\frac{8r_0}{w+l} \right) - 2 \right], \tag{1}$$

where μ_0 denotes the vacuum permeability, r_0 is the mean radius of the resonant ring, w is the width of the metallic strip, and ℓ is the metal thickness. The capacitive behavior, on the other hand, is mainly attributed to the gap between the split ends of the resonator. It can be described as

$$C_e \approx \varepsilon_0 \varepsilon_r \cdot \frac{\pi r_0 \ell}{t}, \tag{2}$$

where ε_0 is the vacuum permittivity, ε_r is the relative permittivity of the surrounding dielectric medium or substrate, and t is the width of the capacitive gap.

The resulting resonance frequency of the metasurface structure is given by

$$f_0 = \frac{1}{2\pi\sqrt{L_e C_e}}. \tag{3}$$

This expression clearly indicates that the resonance frequency is highly sensitive to the effective capacitance C_e, which is influenced by the relative permittivity ε_r of the surrounding environment. In contrast, L_e is primarily determined by the fixed structural parameters. As a result, *the fundamental principle of passive metasurface-based sensing is to modulate ε_r through the interaction between the metasurface and the target material introduced on or near its surface.* This change in ε_r can be interpreted as the addition of an extra capacitance C_1, which modifies the total effective capacitance to $(C_e + C_1)$. Consequently, the perturbed resonance frequency can be expressed as

$$f' = \frac{1}{2\pi\sqrt{L_e(C_e + C_1)}}. \tag{4}$$

By tracking the shift in resonance frequency from f_0 to f', we can infer both the presence and concentration level of the target analyte.

For a bandstop-based passive metasurface, the quality factor (Q factor) is a crucial performance metric used to evaluate the design efficiency of the structure [23, 39]. It is defined as

$$Q = \frac{f_0}{BW}, \tag{5}$$

where f_0 represents the resonant frequency at which the system exhibits a resonance valley characterized by significant attenuation and a sharp dip in the reflection coefficient S_{11}. The bandwidth BW refers to the frequency range for the resonance valley, i.e., the frequency range between the two points where the magnitude of S_{11} is 3 dB larger than the minimum value. This parameter characterizes the sharpness of the resonance, indicating how selectively the system responds around its center frequency. In RF-based wireless sensing applications, especially those employing devices with high-frequency resolution, a higher Q factor implies greater sensitivity of the passive surface to subtle environmental changes. This allows the reflected signal to capture more detailed information within the resonance valley, enabling more accurate detection.

3 PASSIVE METASURFACE CAPSULE UNIT DESIGN

In this section, we detail the design and development of the proposed passive metasurface capsule unit. We begin by investigating how soil moisture and nitrogen concentration jointly influence the electromagnetic response of metasurface-based soil sensing, supported by controlled in-lab experiments. Next, we describe the design principles of the passive metasurface that minimizes underground signal attenuation while maintaining a balanced trade-off between sensing sensitivity and propagation robustness. We then present a novel sandwich-structured metasurface capsule, which mitigates the vulnerability of conventional metasurfaces when directly exposed to soil. Finally, we introduce a consolidated metasurface array that integrates two distinct metasurface designs to enrich soil-related feature encoding within the available UWB bandwidth.

3.1 Characterizing the Effect of Soil Moisture and Nitrogen on Metasurface Response

In this section, we investigate how soil moisture and nitrogen concentration jointly influence the electromagnetic response of the metasurface. We conduct a series of controlled in-lab experiments to characterize how variations in moisture content and nitrogen levels affect the reflection spectrum and resonance behavior. This analysis provides key insights into the underlying sensing mechanism and guides the subsequent metasurface design for robust and accurate soil property estimation.

Analyzing Impact of Moisture on Metasurface.

(a) Upper Soil Box

(b) Lower Soil Box

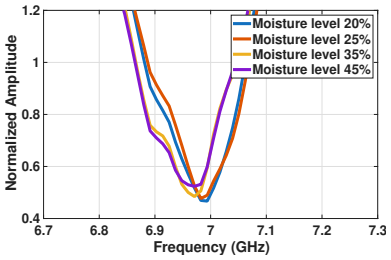

(c) In-lab Moisture Test

Fig. 3. Impact of soil moisture on the metasurface response in controlled lab experiments. The first two subfigures illustrate the in-lab setup: (a) The upper soil box used for radar–metasurface communication without soil filling, and (b) the lower soil box filled with soil under controlled moisture levels that directly contact the metasurface. (c) shows the measured spectral responses under different soil moisture conditions.

First, we investigate the impact of soil moisture on the passive metasurface, as soil moisture plays a dominant role in soil sensing due to its high proportion in soil. Fig. 3(a) and Fig. 3(b) illustrate the controlled in-lab sensing setup, which consists of an upper soil box and a lower soil box.

The upper soil box (Fig. 3(a)) corresponds to the propagation path between the radar and the metasurface and has dimensions of $200 \times 200 \times 120$ mm. To isolate the impact of soil moisture on the metasurface response, the upper box is left unfilled, maintaining a stable direct propagation path between the radar and the metasurface. The lower soil box (Fig. 3(b)) has dimensions of $149.5 \times 59.5 \times 20$ mm and is filled with a fixed soil mass of 50 g. An initial moisture level of 20% is used as the starting condition. Different moisture levels are then obtained by adding appropriate amounts of water, followed by thorough mixing to ensure homogeneous moisture distribution prior to each measurement. The lower box is in direct contact with the ground-facing layer of the metasurface capsule and serves as a controllable dielectric load.

The metasurface capsule has overall dimensions of $130 \times 50.8 \times 9.5$ mm and is mounted at the bottom of the upper box, with an effective communication distance of 30 cm from the UWB radar. A recessed opening of $150 \times 60 \times 2.2$ mm is machined into the bottom surface of the upper box, allowing the lower soil box to be mechanically nested. This nested structure ensures smooth and planar contact between the soil and the ground-facing membrane of the metasurface capsule throughout the experiments.

We observe that identifying and extracting informative spectral features from the reflected signal—such as resonance shifts and amplitude attenuation—can provide valuable insights into soil composition and enable more accurate and robust soil sensing. Given the inherently high moisture content in soil, the presence of water significantly alters the electromagnetic response of the metasurface, leading to pronounced resonance frequency shifts, as shown in Fig. 3(c). When the moisture level in the lower box increases from 20% to 45% [10], a clear frequency shift is observed, indicating strong coupling between moisture variation and the metasurface resonance.

According to Eq. 4, the shifted resonance frequency f_1 can be expressed as

$$f_1 = \frac{1}{2\pi\sqrt{L_e(C_e + C_m)}}, \tag{6}$$

where C_m represents the additional effective capacitance induced by the presence of moisture in the surrounding medium. The total effective capacitance $C_t = C_e + C_m$ is proportional to the effective permittivity ϵ_t of the soil–metasurface composite system. In metasurface-based soil sensing, this frequency-shift phenomenon is

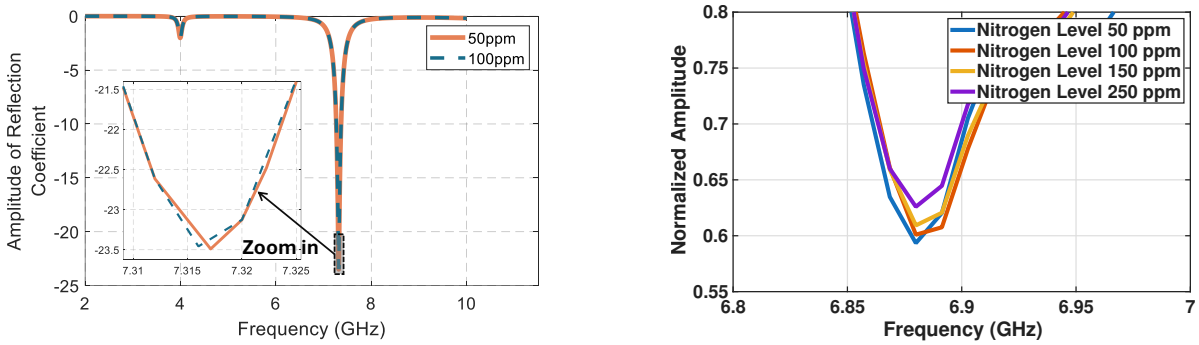

(a) Simulations of Nitrogen

(b) In-lab Nitrogen Test

Fig. 4. Comparison between simulated and in-lab results illustrating the impact of nitrogen on the metasurface response. (a) The simulation demonstrates the expected resonance behavior under varying nitrogen concentration changes. (b) The in-lab measurements show that variations in nitrogen concentration primarily manifest as changes in the resonance amplitude. These consistent patterns support the theoretical model and suggest the feasibility of amplitude-based nitrogen detection.

primarily governed by changes in ϵ_t, as the increasing moisture content elevates the effective permittivity of the soil, leading to a higher overall capacitance and consequently a lower resonance frequency.

Analyzing Impact of Nitrogen on Metasurface. Besides soil moisture, nitrogen is another critical element in soil that is essential for plant growth. However, the concentration of nitrogen is significantly lower than that of moisture, typically around 25–125 ppm after fertilization [2, 37], which is four orders of magnitude smaller than the range of soil moisture content. Most nitrogen in fertilizers converts into nitrate ions (NO_3^-) when dissolved in soil water, and its effect on the metasurface is easily masked by the dominant variations introduced by moisture.

Moreover, the nitrogen concentration itself is insufficient to cause a notable resonance frequency shift. As shown in Fig. 4(a), we simulate the metasurface response under aqueous nitrate solutions with concentrations of 50 ppm and 100 ppm directly contacting the metasurface as a dielectric load. Even under this large concentration difference, the resonance frequency shift remains minimal and nearly indistinguishable. In addition, commercial devices commonly used for daily sensing applications, such as UWB radars [35], provide a limited frequency resolution of approximately 15.6 MHz, making it impractical to detect such small shifts through conventional frequency shift-based sensing methods. Therefore, it becomes necessary to explore a new sensing rationale that enables us to capture the nitrogen-induced effects on the metasurface. In lossy materials, such as conductive aqueous solutions or complex soil mixtures, the electromagnetic response can be characterized by a complex permittivity ε_t [3], which can be decomposed into the real part ε' associated with energy storage and resonance frequency, and the imaginary part ε'' corresponding to energy loss. ε'' is related to the effective electrical conductivity σ_e and can be expressed as: $\varepsilon'' = \frac{\sigma_e}{2\pi f \varepsilon_0}$, where f is the operating frequency and ε_0 is the permittivity of free space.

Furthermore, the attenuation constant α, which quantifies the propagation loss of electromagnetic waves in lossy materials, can be defined as [6]

$$\alpha = \pi f \sqrt{\mu_r \varepsilon_r} \left(\sqrt{1 + \left(\frac{\sigma_e}{2\pi f \varepsilon_r \varepsilon_0} \right)^2} - 1 \right), \tag{7}$$

where μ_r is the relative permeability and ε_r is the relative permittivity of the material. An increase in σ_e leads to a higher α, resulting in stronger attenuation of the electromagnetic wave as it propagates through the medium.

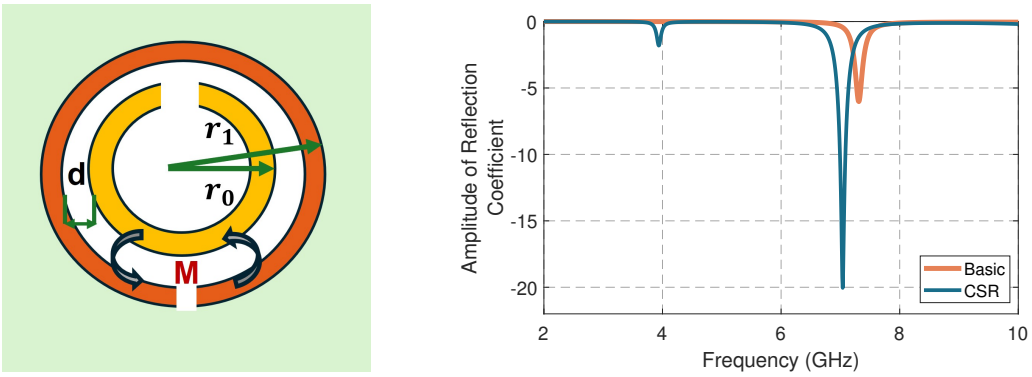

(a) Surface Layer Structure by Leveraging Mutual Coupling

(b) Simulated Reflection Responses Comparing the Basic Structure and the CSR-Based Design

Fig. 5. Design of surface layer structure.

When the nitrate concentration increases after fertilization, σ_e rises accordingly, leading to a higher ε'' and thus greater electromagnetic loss.

To validate this phenomenon, we conducted controlled in-lab experiments to observe nitrogen-induced variations from a new perspective. In this experiment, the soil moisture level was fixed at 55% to eliminate the influence of moisture fluctuations and isolate the effect of nitrogen concentration. As shown in Fig. 4(b), when the nitrogen concentration increases from 50 ppm to 250 ppm, the reflected spectrum exhibits a noticeable reduction in amplitude, while the resonance frequency remains nearly unchanged. This observation further confirms that nitrogen concentration primarily affects the electromagnetic loss, which is manifested as amplitude attenuation, rather than altering the resonance frequency, due to its limited impact on the real part of the effective permittivity.

These results demonstrate that variations in the resonance amplitude can serve as a reliable indicator of nitrate concentration when soil moisture and other environmental factors are controlled. This mechanism is particularly useful in post-irrigation or post-fertilization stages, where monitoring nitrate dynamics is essential for precision soil management. By using the known moisture level as a reference, the nitrate concentration can be quantitatively inferred from the amplitude of the reflected metasurface spectra.

3.2 Passive Metasurface Design

After establishing the sensing rationale of soil moisture and nitrogen, we proceed to design a passive metasurface that achieves a balance between sensing sensitivity and environmental robustness for on-site deployment. The design follows three essential objectives: (1) ensuring moisture sensitivity through both resonance frequency shift and amplitude variation to capture permittivity and loss changes caused by moisture; (2) maintaining nitrogen sensitivity through amplitude modulation, since nitrate ions primarily affect the imaginary part of permittivity; and (3) preserving robustness against underground attenuation, so that the reflected signal remains detectable despite propagation loss and scattering. These objectives together ensure that the proposed metasurface remains both sensitive to soil composition and resilient under real-world conditions.

By meeting these design objectives, the passive metasurface can achieve accurate soil monitoring while maintaining sufficient signal integrity for ground-based radar reception, even in challenging underground propagation environments. To realize this, we implement a two-step metasurface design approach.

Step 1: Baseline Single-Ring Design. We first establish a baseline design by applying the theoretical formulations in Equation (1) and Equation (2) to ensure that the initial resonance frequency f_0 falls within the operational frequency range of the UWB radar device (centered at 7.29 GHz with a 1.4 GHz bandwidth)

$$f_0 = \frac{1}{2\pi}\sqrt{\frac{t}{\mu_0\varepsilon_0\varepsilon_r\pi r_0^2\ell\left(\ln\left(\frac{8r_0}{w+\ell}\right)-2\right)}}, \quad (6.59\ \text{GHz} \le f_0 \le 7.99\ \text{GHz}). \tag{8}$$

This expression shows that the resonance frequency f_0 is jointly determined by the resonator's geometrical parameters (r_0, w, ℓ, t) and the effective permittivity ε_r of the surrounding medium. Increasing the mean radius r_0 decreases the resonance frequency by enlarging both inductance and capacitance, while increasing the metallic strip width w or the gap width t raises f_0 by reducing inductance or capacitance, respectively. The metal thickness ℓ is fixed by fabrication constraints, whereas ε_r varies dynamically with surrounding soil conditions.

During the design process, we adopt a hierarchical tuning strategy for the single split-ring structure. The mean radius r_0 is first coarsely adjusted to bring the resonance within the target frequency range, followed by fine-tuning of the strip width w to optimize the quality factor Q and ensure precise frequency alignment. The gap width t is kept constant to maintain stable capacitive coupling. This hierarchical approach balances coarse and fine control, ensuring both frequency accuracy and manufacturability. Through this tuning process, the metasurface achieves high sensitivity to soil property variations, establishing the foundation for effective sensing.

Step 2: Dual-Ring CSR Design. To deepen the resonance valley and enhance the distinguishability of the reflected signal, we incorporate an additional split ring into the surface layer, forming a dual-ring complementary split-ring (CSR) structure. In this configuration, the mutual coupling between the two concentric rings significantly shapes the overall resonance behavior. As illustrated in Fig. 5(a), the CSR can be modeled as an LC resonator that includes both self-inductance and mutual inductance M between rings, approximated as [6, 8]

$$M \approx \mu_0\sqrt{r_1 r_2}\left[\ln\left(\frac{8\sqrt{r_1 r_2}}{d}\right)-2\right], \tag{9}$$

where r_1 and r_2 are the mean radii of the outer and inner rings, and d is the spacing between them. The total effective inductance of the coupled system is given by

$$L_{\text{total}} = L_1 + L_2 + 2M. \tag{10}$$

While electric-field coupling introduces a mutual capacitance C_m, its effect is negligible within the frequency band of UWB radar because the inter-ring spacing exceeds 0.3 mm in our design. Therefore, the resonance frequency of the dual-ring CSR structure can be expressed as

$$f_m = \frac{1}{2\pi\sqrt{L_{\text{total}}C_e}}. \tag{11}$$

Stronger coupling (larger M) increases L_{total} and thus lowers f_m. The coupling strength is primarily governed by the distance d between the two rings. By tuning d, the resonance characteristics can be precisely controlled to meet the desired operational bandwidth. For passive underground soil sensing, it is essential to align f_m with the radar's central frequency to maximize signal distinguishability and sensitivity. Fig. 5(b) compares the simulated responses of the baseline and CSR designs. The CSR configuration yields a resonance frequency of 7.04 GHz with an attenuation of −20 dB, providing adequate design flexibility for further optimization of the metasurface capsule in subsequent sections.

While the CSR-based design results in deeper resonance valleys, its primary advantage lies not in increased attenuation alone, but in improved signal distinguishability across different soil conditions. As illustrated in Fig. 5, the CSR configuration increases the separation between resonance amplitudes corresponding to different moisture or nitrogen levels. This enhanced amplitude separation reduces spectral overlap between conditions, making the reflected signals more distinguishable in the presence of measurement noise and soil heterogeneity.

Improved amplitude separation directly benefits downstream inference by providing more discriminative spectral features for both signal reconstruction and regression. This effect is particularly important for nitrogen sensing, where relatively weak nitrogen-induced spectral variations are often masked by dominant moisture effects in conventional metasurface designs.

3.3 Encapsulated Metasurface Capsule Design

Previous metasurface designs provide a feasible solution for soil moisture and nitrogen sensing. However, the design process primarily focuses on optimizing the surface-layer geometry and dielectric parameters to achieve high sensitivity, while overlooking potential environmental impacts during real-world deployment. Direct contact between the metasurface and soil may significantly alter its electromagnetic response, compromising the stability and repeatability of sensing performance.

When the metasurface is directly buried in soil, the surface layer interacts with the soil medium, disturbing the designed electromagnetic field distribution. This direct contact modifies the effective permittivity around the resonant elements and randomly shifts key parameters such as resonance frequency and attenuation, leading to unpredictable deviations in the spectrum of reflected signal.

To accurately evaluate this underground sensing scenario, we perform a comparative simulation by adding a 10 mm soil layer in direct contact with the metasurface's top surface. The soil is modeled with a relative permittivity of $\varepsilon_r = 5.5$ and a loss tangent of $\tan\delta = 0.08$, assumed to be constant across the 2–10 GHz range. Frequency dispersion effects are neglected due to the soil's relatively stable dielectric behavior within this band. As shown in Fig. 6(a), compared with the free-space result (yellow curve), direct soil contact (dark curve) drastically alters the metasurface's electromagnetic behavior: the original resonance peak disappears and the overall attenuation decreases, indicating that the metasurface can no longer operate reliably without proper encapsulation.

To quantitatively analyze this degradation, the reflection coefficient Γ at the metasurface–soil interface is defined as [49]

$$\Gamma = \frac{Z_{\text{meta}} - Z_{\text{soil}}}{Z_{\text{meta}} + Z_{\text{soil}}}, \tag{12}$$

where Z_{meta} is the effective surface impedance of the metasurface, and Z_{soil} denotes the intrinsic impedance of the surrounding soil. Therefore, when Z_{meta} and Z_{soil} are close, a large portion of the incident energy penetrates into the lossy soil rather than being reflected, resulting in signal distortion and loss of resonance visibility.

Previous work [12] mitigated this issue by placing a large tube between the on-ground radar and the underground metasurface to create a direct path. However, such a configuration is impractical for large-scale agricultural deployment as it occupies surface space and obstructs plant growth. To overcome this limitation, we design a compact encapsulated metasurface capsule that introduces an air layer and a thin protective cover above the metasurface. The top cover is fabricated using Polyethylene Terephthalate Glycol-modified (PETG), a cost-effective and biodegradable polymer with excellent electromagnetic transparency and low dielectric loss [25]. Its mechanical rigidity protects the metasurface pattern from soil pressure without degrading RF propagation. Compared with other 3D-printable materials such as PLA, PETG offers a favorable balance among structural strength, RF compatibility, and long-term environmental stability, making it a suitable encapsulation material for battery-free, soil-deployable sensing systems.

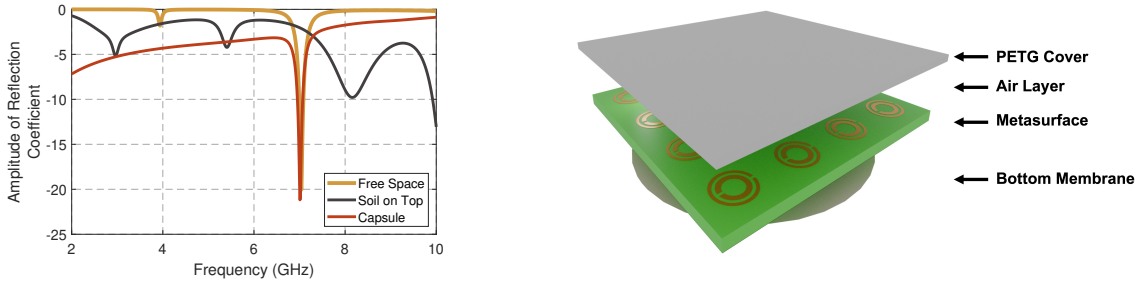

(a) Impact of Soil and Capsule Structure

(b) 3D Model of the Encapsulated Metasurface Capsule

Fig. 6. (a) Simulated impact of soil contact and encapsulation on metasurface performance. The direct-contact case (dark curve) exhibits degraded resonance behavior, whereas the proposed capsule design (red curve) mitigates this degradation and yields a reflection spectrum comparable to the free-space condition (yellow curve). (b) 3D model of the PETG–PTFE encapsulated metasurface capsule. The top PETG layer provides mechanical protection and air insulation, while the bottom hydrophilic PTFE membrane facilitates stable soil–metasurface interaction for consistent sensing.

As shown in Fig. 6(a), the proposed capsule structure (red curve) effectively confines the electric fields near the metasurface and stabilizes the reflection coefficient Γ to a level comparable to the free-space condition. This ensures that the reflected signal remains both detectable and informative for on-ground radar reception.

Beyond soil interference, underground environments also contain irregular objects such as stones, metallic debris, or dense aggregates that can act as random electromagnetic loads on the ground layer of the metasurface. Although they may not completely disable the sensor, such irregularities can introduce significant spectral noise and prediction deviations. To mitigate these effects, a hydrophilic polytetrafluoroethylene (PTFE) membrane is introduced at the bottom of the capsule. The PTFE membrane serves as an intermediate interface that collects soil properties—such as moisture and nitrate content—and transfers them to the metasurface through stable and consistent dielectric coupling. This layer effectively filters high-frequency environmental fluctuations while maintaining sensitivity to slow-varying changes in soil composition.

By jointly considering the electromagnetic impact of both encapsulation materials and the surrounding soil medium, the proposed capsule design preserves sufficient spectral bandwidth for detecting frequency and amplitude variations while maintaining signal robustness under long-term underground deployment.

3.4 Consolidated Dual-resonator Array

After accounting for environmental impacts in in-situ deployment, SoilNutri has evolved into a feasible solution for real-world soil sensing applications. However, accurately characterizing the joint influence of soil moisture and nitrogen concentration remains challenging for a single-resonance metasurface array. Although a single resonator can generate a resonance valley containing multiple high-sensitivity points in the frequency spectrum, the limited number of distinct resonance features makes it difficult to decouple the coupled effects of moisture and nitrogen.

Inspired by the wide operational bandwidth of UWB radar, we design a *Consolidated Dual-Resonator Array* that integrates two metasurface units with distinct resonance characteristics. This hybrid configuration increases the number of high-sensitivity frequency points, leading to a richer spectral representation that improves parameter separability and enhances prediction accuracy. In this design, one resonator is primarily tuned to respond to permittivity variations caused by soil moisture, which appear as resonance frequency shifts, while the other exhibits higher sensitivity to conductivity-related amplitude attenuation induced by nitrogen ions. Instead of relying on a single absolute spectral response, SoilNutri utilizes the relative spectral relationship between the

two metasurface units, capturing both invariant and differential patterns between their reflected spectra. By analyzing these relative features, the nitrogen-induced amplitude variations can be isolated from moisture-related frequency shifts. This differential spectral mechanism introduces a self-calibrating property, allowing the first resonator to act as a reference baseline that dynamically compensates for soil moisture fluctuations and thus enhances robustness under diverse environmental conditions.

During signal propagation, the reflected UWB signal from the dual-resonator metasurface can be modeled as the superposition of reflections from both resonant units. Each resonator contributes a unique frequency-dependent reflection coefficient, and the total reflection $\Gamma_{\text{dual}}(f)$ can be expressed as

$$\Gamma_{\text{dual}}(f) = \Gamma_1(f) + \Gamma_2(f)e^{-j2\pi f\Delta\tau}, \tag{13}$$

where $\Gamma_1(f)$ and $\Gamma_2(f)$ represent the complex reflection coefficients of the first and second resonators, and $\Delta\tau$ denotes the effective time delay corresponding to the spatial separation between them. Each $\Gamma_i(f)$ can be approximated as a Lorentzian-type resonant response [42]

$$\Gamma_i(f) = \frac{A_i}{1 + jQ_i\left(\frac{f}{f_{0i}} - \frac{f_{0i}}{f}\right)}, \tag{14}$$

where f_{0i} and Q_i denote the resonant frequency and quality factor of the ith resonator, and A_i is an amplitude scaling term determined by the impedance contrast between the metasurface and its surrounding soil medium.

By analyzing both the absolute and relative variations between $\Gamma_1(f)$ and $\Gamma_2(f)$ across the frequency domain, the system captures complementary spectral features. The resonance frequency shift primarily reflects permittivity changes associated with soil moisture, while amplitude modulation encodes conductivity variations induced by nitrogen ions. This co-resonant configuration enriches the information content of the reflected spectrum and strengthens the system's capability to decouple these two physical effects in subsequent signal processing stages.

To validate this concept, we fabricated the consolidated dual-resonator metasurface array and characterized its spectral behavior under laboratory conditions. The real fabricated structure and the measured combined spectrum are shown in Fig. 7(a) and Fig. 7(b), respectively. The central hole in the fabricated metasurface structure is reserved for an auxiliary physical indicator, which will be introduced in detail in Sec. 4. The two metasurface units within the array exhibit distinct electromagnetic responses that jointly contribute to the overall spectral richness. As illustrated in Fig. 7(b), two main resonance feature regions can be identified. *Feature Region 1* serves as the dominant region for moisture sensing, where both frequency shift and amplitude attenuation are primarily driven by variations in soil permittivity. In contrast, *Feature Region 2* provides a complementary spectral reference that supports the construction of relative spectral relationships between the two resonators, enabling isolation of nitrogen-induced amplitude attenuation while minimizing interference from moisture fluctuations.

By establishing this dual-feature framework, the consolidated design provides a physically interpretable sensing basis and creates a direct linkage between structural resonance characteristics and frequency-domain spectral responses. This hardware foundation supports the subsequent signal processing module, which extracts, reconstructs, and interprets these rich spectral features for accurate soil sensing, as detailed in Sec. 4.

4 SIGNAL PROCESSING FOR SOIL MOISTURE AND NITROGEN SENSING

Building upon the hardware foundation established by the consolidated dual-resonator metasurface, this section details the signal processing workflow of SoilNutri, as illustrated in Fig. 8. The goal of this module is to extract, reconstruct, and interpret the rich spectral information encoded in the radar-reflected signals, enabling accurate estimation of soil moisture and nitrogen concentration.

After the UWB radar transmits and receives reflections from the underground metasurface capsule, SoilNutri first converts the time-domain waveform into its frequency-domain representation via a Fast Fourier Transform

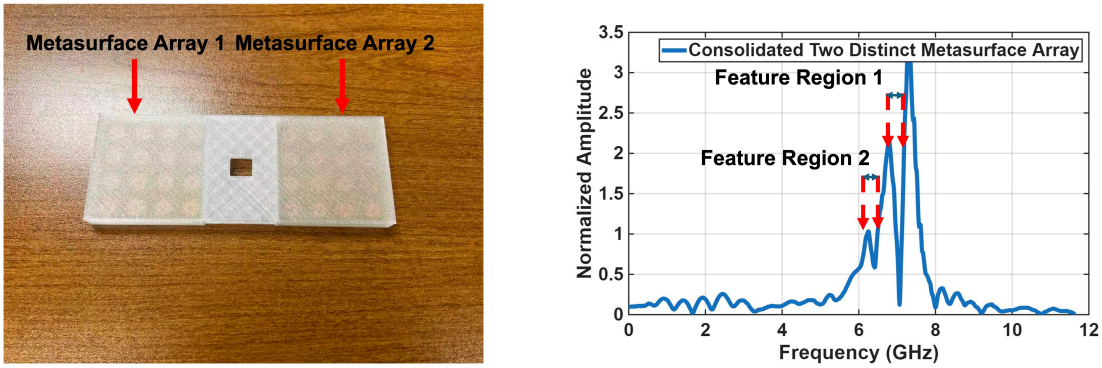

(a) Fabricated Consolidated Metasurface Array

(b) Measured Combined Spectral Features

Fig. 7. (a) Fabricated prototype of the consolidated dual-resonator metasurface array, consisting of two metasurface units with distinct resonance characteristics. (b) Measured frequency spectrum showing two separated resonance feature regions. Feature Region 1 primarily reflects soil moisture effects (frequency shift and amplitude attenuation), whereas Feature Region 2 captures relative spectral variations that enable nitrogen-specific amplitude identification.

(FFT). An auxiliary 3D-printed alignment rod is used to maintain a consistent spatial orientation between the radar and the metasurface, minimizing variations introduced by angular misalignment or uneven placement. To further enhance the discriminative power of the spectrum, a frequency-derivative operation is applied to the amplitude responses, amplifying compositional sensitivity while suppressing large-scale attenuation, thereby producing a robust feature representation for subsequent modeling.

Building on these extracted spectral features, SoilNutri employs a two-stage generative learning framework to recover and interpret the latent spectral information underlying soil properties. In *Stage I*, a β-VAE is pre-trained under controlled laboratory conditions to learn the intrinsic mapping from the degraded soil spectrum S to its clean reference N_0, forming a domain-invariant latent representation that captures the stable amplitude correlation between the twin resonators. In *Stage II*, the pre-trained encoder E_ϕ is integrated into a shared-latent multi-task network for field deployment, where spectral reconstruction and nutrient prediction are jointly optimized through a composite loss that combines reconstruction consistency, moisture/nitrogen regression, derivative smoothness, and valley-aware regularization. This hierarchical training paradigm enables SoilNutri to effectively bridge laboratory pre-training and real-world adaptation, achieving noise-resilient and generalizable sensing across different soil types, depths, and deployment conditions.

4.1 Spectrum Information Extraction

Building on the hardware foundation described in Sec. 3, we next focus on extracting spectral features from the reflected radar signal captured by the dual-resonator metasurface array. The UWB radar first performs channel estimation on the received underground reflected signal and derives the channel impulse response (CIR) $p(t)$. By applying a Fourier transform to the CIR, the system obtains the frequency response $H(f)$ of the channel, given as [13, 31]

$$H(f) = \int_{-\infty}^{\infty} p(t) e^{-j2\pi f t} dt = |H(f)| e^{j\phi(f)}, \tag{15}$$

where $|H(f)|$ and $\phi(f)$ denote the magnitude and phase components of the frequency response, respectively. The magnitude spectrum $|H(f)|$ serves as a robust feature that reflects the combined influence of the metasurface, soil composition, and propagation environment.

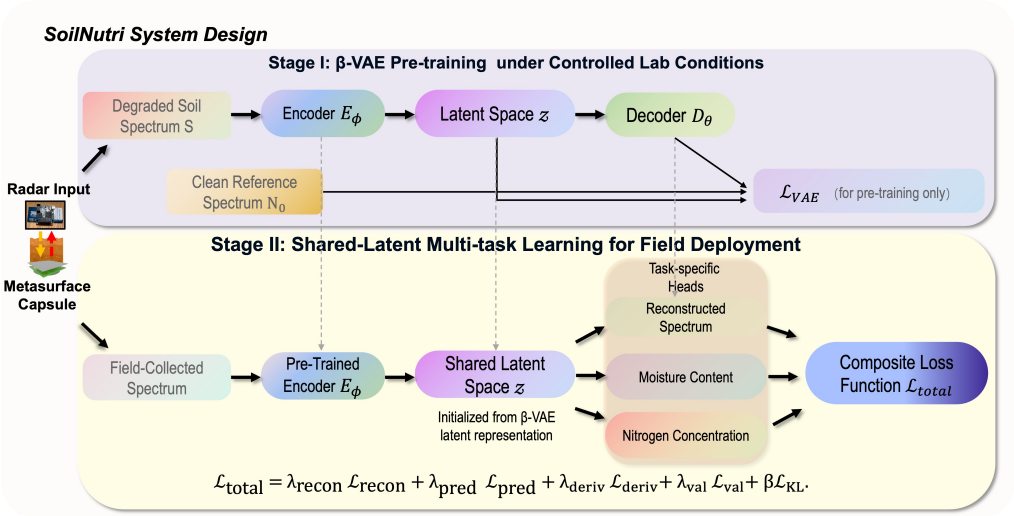

Fig. 8. SoilNutri signal processing framework. Stage I pre-trains a β-VAE under controlled lab conditions to reconstruct the clean reference spectrum N_0 from the degraded soil reflection S, forming a domain-invariant latent representation. Stage II fine-tunes the pre-trained encoder within a shared-latent multi-task network, jointly optimizing spectral reconstruction, moisture and nitrogen regression, derivative smoothness, and valley-aware regularization through the composite loss $\mathcal{L}_{\text{total}}$.

Auxiliary Physical Indicator and Derivative Feature. For practical field deployment, an auxiliary physical indicator is integrated above the metasurface capsule to assist in alignment between the UWB radar and the metasurface array, as shown in Fig. 9(a). The indicator is fabricated from the same PETG material to ensure electromagnetic transparency and structural compatibility, with an essential length of 15 cm and multiple adjustable segments of 20 cm to accommodate different soil depths and radar installation heights. Its hollow rectangular structure provides a clear reference axis for aligning the radar beam with the center of the metasurface, ensuring consistent positioning during repeated measurements.

While the indicator effectively maintains spatial position between the radar and the metasurface, it inevitably introduces an additional soil-irrelevant reflection path. To quantitatively assess its electromagnetic influence on the sensing spectrum, we conduct a controlled in-lab measurement to evaluate how the indicator modifies the reflected signal characteristics. As illustrated in Fig. 9(b), this extra reflection slightly alters the spectral response by causing minor frequency shifts and amplitude perturbations in the dominant resonance region.

To mitigate the interference introduced by these irrelevant propagation components, SoilNutri computes the first-order derivative of the amplitude spectrum with respect to frequency $\frac{d|H(f)|}{df}$. Since the metasurface-induced response typically introduces localized and abrupt frequency-dependent variations, the derivative operation suppresses constant or slowly varying background components, effectively isolating informative resonance-related changes. As shown in Fig. 9(c), the derivative spectrum exhibits a much more stable pattern compared to the raw amplitude spectrum, thereby improving robustness against environmental noise and unrelated underground reflections. This feature extraction process provides a reliable input representation for the subsequent reconstruction and multi-task learning modules described in Section 4.

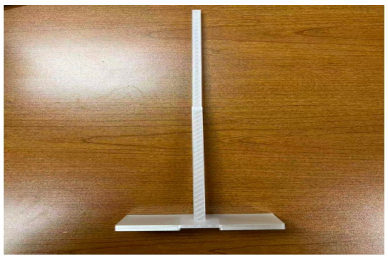

(a) Auxiliary Physical Indicator Alignment Setup

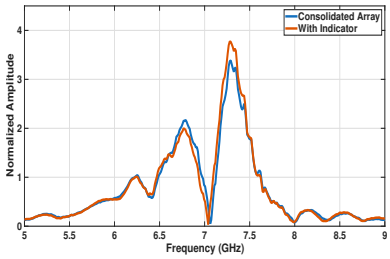

(b) Amplitude Spectrum with Indicator Effect

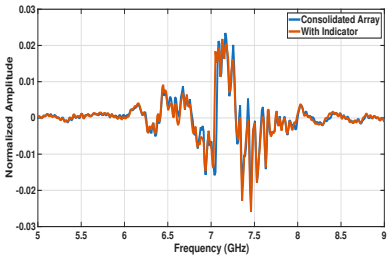

(c) Derivative Spectrum for Noise Suppression

Fig. 9. (a) Laboratory setup showing the auxiliary physical indicator used to ensure consistent alignment between the UWB radar and the metasurface capsule. (b) Measured amplitude spectrum showing slight distortions caused by the additional reflection path introduced by the indicator. (c) First-order derivative of the amplitude spectrum, which effectively suppresses background fluctuations and stabilizes resonance-related variations for subsequent signal processing.

(a) Normal Soil (b) Bonsai Soil (c) Peatmoss Soil (d) Compost Soil

Fig. 10. Four representative in-lab soil types used for controlled pre-training experiments: (a) normal soil, (b) bonsai soil, (c) peatmoss soil, and (d) compost soil. These samples differ in organic content, porosity, and moisture-retention capacity, enabling comprehensive evaluation across diverse soil compositions.

4.2 Stage I: Spectral Reconstruction via β-VAE Information Recovery

To recover the intrinsic reflection characteristics of the metasurface that are distorted by soil attenuation, SoilNutri employs a β-Variational Autoencoder (β-VAE) [40] trained under controlled in-lab conditions. The pre-training stage aims to establish the intrinsic mapping $S \rightarrow N_0$, where S denotes the degraded soil-reflected spectrum and N_0 represents its clean free-space reference. By modeling the statistical dependency between amplitude and phase spectra, β-VAE captures invariant electromagnetic features that are stable across environmental diversities.

In-lab Dataset and Setup. Four representative soil types—normal, bonsai, peatmoss, and compost—are employed to capture a broad range of dielectric and compositional diversity (Fig. 10). *Normal soil* consists of a balanced mixture of sand, silt, and clay, representing a standard loam texture. *Bonsai soil* contains a higher fraction of inorganic particles such as akadama and pumice, featuring low organic content and fast drainage. *Peatmoss soil* is rich in organic matter and exhibits high porosity and water retention, whereas *Compost soil* contains decomposed plant residues with abundant nutrients and moderate conductivity. These controlled samples cover a wide range of permittivity, moisture-holding capacity, and nutrient concentration. To ensure compatibility with field deployments, the in-lab dataset further spans multiple *moisture levels* (15–60%), *radar-to-metasurface distances* (15–75 cm), and variable packing densities, providing the β-VAE with diverse training conditions to learn a domain-invariant latent representation.

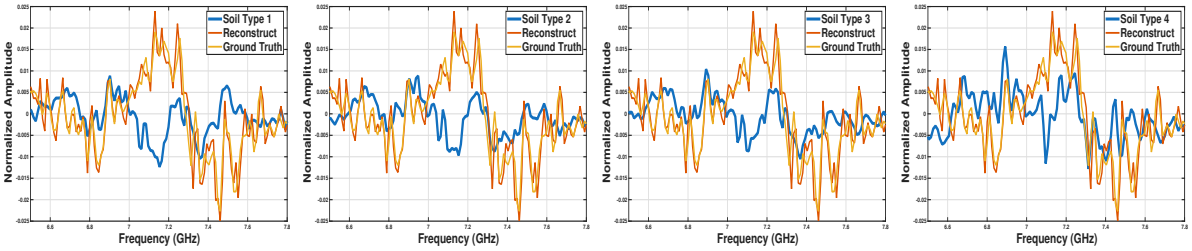

(a) Normal Soil (b) Bonsai Soil (c) Peatmoss Soil (d) Compost Soil

Fig. 11. Comparison between the original measured spectra and the β-VAE reconstructed spectra across four in-lab soil types. The reconstructed spectra preserve the major resonance-valley patterns observed in the measurements, indicating consistent reconstruction performance across different soil compositions.

Model Formulation. Given an input spectrum $\mathbf{x}_S$, the encoder $E_\phi(\cdot)$ projects it into a latent representation $\mathbf{z} \sim q_\phi(\mathbf{z}|\mathbf{x}_S)$, and the decoder $D_\theta(\cdot)$ reconstructs its clean counterpart $\hat{\mathbf{x}}_{N_0} = D_\theta(\mathbf{z})$. The training objective combines a reconstruction term and a Kullback–Leibler (KL) divergence regularizer

$$\mathcal{L}_{\text{VAE}} = \|\mathbf{x}_{N_0} - \hat{\mathbf{x}}_{N_0}\|_2^2 + \beta\, D_{\text{KL}}\big(q_\phi(\mathbf{z}|\mathbf{x}_S) \,\|\, p(\mathbf{z})\big), \tag{16}$$

where β controls the strength of latent regularization, promoting disentanglement between environment-dependent noise and the domain-invariant amplitude–phase correlations of the twin resonators.

Through this pre-training process, the encoder learns a physically grounded and transferable latent space that captures the intrinsic electromagnetic response of the metasurface while suppressing soil-induced distortions. As shown in Fig. 11, the reconstructed spectra maintain stable valley positions and consistent amplitude patterns across all soil types, validating β-VAE's ability to recover invariant reflection characteristics.

Compared with other generative learning architectures such as diffusion models [19, 34], masked autoencoders [18], GAN-based approaches [17], and convolutional neural networks [36] (CNNs), the β-VAE offers a favorable balance between reconstruction accuracy and training efficiency. Its lightweight structure and disentangled latent design significantly reduce computational overhead while maintaining high data-imputation fidelity. These characteristics make β-VAE particularly suitable for edge-oriented sensing applications, where limited hardware resources and real-time operation are essential considerations.

This latent representation is subsequently used to initialize the shared-latent multi-task network introduced in Stage II, forming the foundation for field-level spectral reconstruction and nutrient prediction. By integrating this pre-trained encoder with newly added reconstruction and regression heads, SoilNutri jointly refines both the spectral restoration and nutrient estimation objectives under real soil conditions, enabling end-to-end optimization across heterogeneous environments.

4.3 Stage II: Multi-task Recognition with Shared-latent Learning

Initialized from the pre-trained β-VAE latent representation, the encoder E_ϕ is incorporated into a shared-latent multi-task framework that jointly optimizes spectral reconstruction and soil property prediction using field-collected data. During fine-tuning, both the encoder and decoder remain trainable to enable adaptive domain alignment, while multiple task-specific heads are appended to the latent embedding $\mathbf{z}$ for regression and auxiliary supervision.

The overall objective integrates reconstruction, prediction, and physical regularization terms as

$$\mathcal{L}_{\text{total}} = \lambda_{\text{recon}}\mathcal{L}_{\text{recon}} + \lambda_{\text{pred}}\mathcal{L}_{\text{pred}} + \lambda_{\text{deriv}}\mathcal{L}_{\text{deriv}} + \lambda_{\text{val}}\mathcal{L}_{\text{val}} + \beta\mathcal{L}_{\text{KL}}, \tag{17}$$

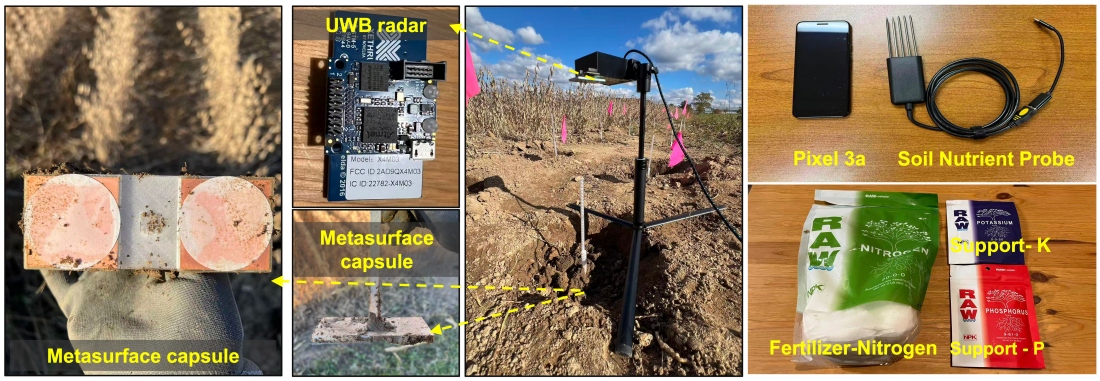

Fig. 12. Default experimental setup and on-site devices used in soil sensing experiments, including the metasurface capsule, UWB radar, and field deployment configuration. The setup also incorporates a commercial soil nutrient probe and a mobile phone for data collection and storage. Nitrogen fertilizer is used as the primary nutrient of interest in the evaluation, while phosphorus- and potassium-based fertilizers are included as supplementary reference materials to control the total fertilization level.

where $\mathcal{L}_{\text{recon}}$ enforces spectral consistency between reconstructed and measured spectra, $\mathcal{L}_{\text{pred}}$ represents regression losses for soil moisture and nitrogen concentrations, $\mathcal{L}_{\text{deriv}}$ preserves local smoothness in amplitude–phase derivatives to suppress spectral noise, and $\mathcal{L}_{\text{val}}$ introduces valley-aware regularization that stabilizes resonance valley locations under soil variability. The final term $\mathcal{L}_{\text{KL}}$ maintains the latent distribution regularization inherited from the pre-trained β-VAE.

Rationale for Composite Optimization. These objectives are complementary rather than conflicting: the reconstruction branch restores full-band spectral fidelity, providing richer gradients for the prediction heads, while the regression branch introduces task-driven supervision that guides the latent representation toward physically interpretable patterns. The derivative and valley-aware terms act as physics-informed regularizers that reduce overfitting and improve spectral stability across soil types. By jointly optimizing all components in a single end-to-end framework, SoilNutri benefits from cross-task regularization, smoother convergence, and enhanced generalization to unseen environmental conditions.

Training Efficiency and Deployment Feasibility. Despite incorporating multiple loss components, the shared-latent framework maintains lightweight training overhead. The model consists of fewer than 1.2 M parameters—an order of magnitude smaller than diffusion or masked autoencoder architectures—requiring only 1.3 GB of GPU memory and converging within 30 epochs on a single NVIDIA A100. The forward pass of the final model takes less than 25 ms on a Jetson Orin NX, demonstrating its suitability for on-device or edge-assisted soil monitoring. Compared with larger generative models, the β-VAE backbone ensures efficient latent encoding while preserving high imputation accuracy, enabling SoilNutri to achieve an effective balance between reconstruction precision and deployability.

Each prediction head consists of a lightweight fully connected block with layer normalization and ReLU activations, forming an AmpNet-style regression structure that efficiently maps the latent embedding to continuous soil parameters. By jointly optimizing reconstruction and prediction tasks within a unified latent space, SoilNutri promotes feature completeness, mitigates environmental noise sensitivity, and achieves robust generalization across diverse soil types, depths, and deployment conditions.

5 IMPLEMENTATION

This section presents the implementation of the SoilNutri prototype.

Metasurface Capsule. The metasurface capsule features an overall dimension of 130 mm × 50.8 mm × 9.5 mm, integrating a consolidated metasurface array within a compact enclosure, as illustrated in Fig. 12. An auxiliary 3D-printed alignment rod is attached to the capsule, with a base length of 15 cm and multiple adjustable extensions of up to 20 cm, enabling flexible deployment across varying soil depths. This compact and modular design allows for effortless underground installation with minimal disturbance to surrounding roots or plant growth during the cultivation period. The total material cost of the metasurface capsule is approximately $1, including $0.20 for the metasurface array fabrication, $0.50 for the commercial hydrophilic membrane, and $0.30 for the PETG top cover produced via 3D printing.

Metasurface. To support low-cost, long-term on-site deployment, the passive metasurface component of SoilNutri is fabricated using a double-sided, 1-oz copper PCB board with an FR4 substrate. The FR4 substrate has a nominal thickness of 1.6 mm.

Membrane. The hydrophilic polytetrafluoroethylene (PTFE) membrane is a chemically modified version of conventional PTFE, providing strong water wettability while maintaining excellent chemical inertness and thermal stability. The hydrophilic treatment enables water and aqueous solutions to readily permeate through the membrane, making it ideal for stable fluid interaction with the surrounding soil environment while minimizing additional interference.

Fabrication Process. The metasurface capsule is assembled in a layered manner. First, the passive metasurface arrays are integrated with the 3D-printed PETG top cover. The top cover provides a uniform thickness of 0.5 mm above the metasurface, balancing mechanical protection with minimal signal degradation. An air layer of 6.4 mm is maintained between the metasurface and the PETG cover to preserve the designed electromagnetic response. Each metasurface array has dimensions of 50 × 50 × 1.6 mm and fits precisely within the top cover. To ensure mechanical robustness under underground conditions, the metasurface arrays are fixed in place using waterproof adhesive. Next, a hydrophilic PTFE membrane is bonded to the ground-facing side of the metasurface, forming a stable interface between the metasurface and the surrounding soil. Finally, an auxiliary physical indicator is attached to the assembled capsule to facilitate physical alignment during deployment.

UWB Device. We employ the Novelda X4M03 ultra-wideband (UWB) radar [35] module as the primary transceiver for signal acquisition. The X4M03 module operates in the 6.0–8.5 GHz frequency band and provides high temporal resolution with sub-centimeter accuracy. It integrates a pair of wideband antennas, a low-noise front-end, and a digital signal processor capable of real-time envelope and phase extraction. During the experiments, the radar is mounted above the metasurface capsule and connected to a laptop via USB for synchronized data acquisition and control using Novelda's XeThru software interface.

Software. All electromagnetic simulations for the metasurface and surrounding soil environment are conducted using CST Studio Suite [1]. MATLAB and Python are utilized for data collection, signal processing, and machine learning model development.

6 EVALUATION

This section presents a comprehensive evaluation of SoilNutri under diverse field conditions. We begin by describing the experimental setup and dataset, followed by the overall prediction performance for soil moisture and nitrate–nitrogen, based on 900 individual on-site measurements. We then analyze the system's robustness under different deployment factors, including burial depth, radar height, and radar-holder angle, as well as its cross-scenario generalization across seasons and environments. Finally, we examine the influence of total soil

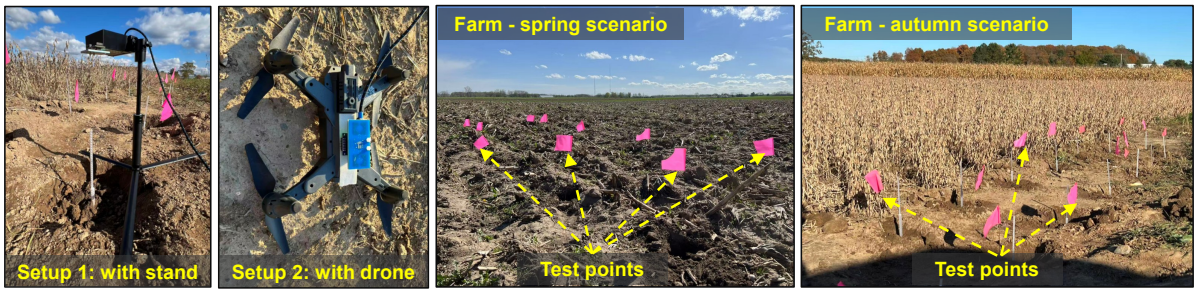

Fig. 13. Experimental setups and field scenarios in the organic farm. (Left) Two radar deployment configurations: Setup 1 with a tripod-mounted radar and Setup 2 with a drone-mounted radar for flexible data collection across the field. (Right) On-site measurements in spring (pre-growth) and autumn (post-harvest) farm scenarios, where pink flags indicate the test locations of buried metasurface capsules.

fertility on nitrogen sensing selectivity and conduct ablation studies to quantify the benefits of joint multi-task optimization and gradient feedback.

6.1 Evaluation Setup and Metric

In this section, we evaluate the performance of SoilNutri through a series of field deployments conducted under varying environmental and seasonal conditions. Two representative environments are considered. The first is a backyard garden, which serves as a controlled setting for small-scale monitoring scenarios such as home gardens or research plots. The second is a large organic farm covering approximately 15,000 m^2, as illustrated in Fig. 13, representing a realistic large-scale agricultural deployment. For the organic farm experiments, we conducted measurements across two distinct growing seasons, spring and autumn, to capture variations in soil conditions before and after plant growth (soybeans), as shown in Fig. 13.

There are two approaches for collecting the reflected signals from the underground metasurface capsules. As shown in Fig. 12, one method involves mounting the UWB radar module on a standard tripod and manually moving the tripod across the monitoring area. Alternatively, the radar can be integrated with a UAV, as shown in Fig. 13, enabling large-scale automated monitoring across expansive farmland areas. In both tripod-based and UAV-assisted deployments, the radar module is aligned with the auxiliary physical indicator of the metasurface capsule to ensure consistent positioning and measurement geometry across data collection sessions.

In the UAV-assisted setup, the radar measurements are collected while the UAV hovers at discrete locations above the buried metasurface capsules, rather than during continuous flight. Data acquisition is performed only during hovering to ensure a stable measurement geometry and to avoid significant motion-induced Doppler effects [46, 48] or spectral distortion.

Device and Support Materials. During the experimental process, we employ a soil nutrient probe, as illustrated in Fig. 12, to collect the reference measurements of soil moisture and nitrogen concentration. In addition, the probe provides supplementary information on soil properties such as temperature, effective permittivity, and the concentrations of phosphorus and potassium. We note that the nitrogen readings provided by commercial soil probes are not ion-specific and are typically derived from conductivity-based estimates. As a result, these measurements are subject to cross-sensitivity to other dissolved ions, soil salinity, and temperature variations, and may exhibit measurement uncertainty or calibration drift under heterogeneous soil conditions. A Google Pixel 3a smartphone is used to interface with the probe and record the sensed data through its companion application.

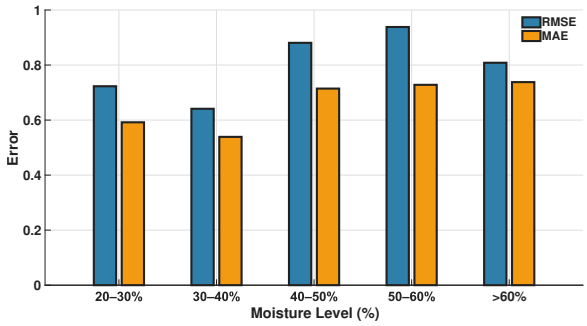

Fig. 14. Moisture prediction (RMSE across ranges).

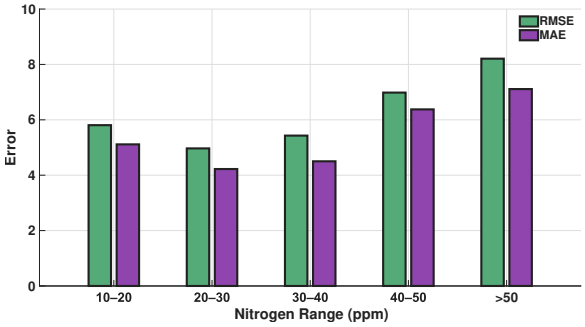

Fig. 15. Nitrogen prediction (RMSE across ranges).

To maintain balanced soil nutrient conditions, three types of fertilizers are used, with nitrogen serving as the primary variable and potassium and phosphorus as supporting elements.

Metric. In the evaluation of soil moisture prediction performance, we adopt two standard regression metrics: Root Mean Squared Error (RMSE) and Mean Absolute Error (MAE). For nitrogen concentration prediction, regression accuracy is adopted as the primary evaluation metric. We focus on achieving *ppm-level* prediction accuracy [37], enabling fine-grained monitoring of soil nutrient dynamics and early detection of nitrogen imbalance or leaching risks. Such precision is essential, as even minor variations in nitrate concentration can significantly influence crop growth and groundwater quality.

6.2 On-site Evaluation of Moisture and Nitrogen Monitoring

In the on-site evaluation, we conduct field experiments across 23 soil pots with varying nutrient and moisture conditions, with a total of 900 individual measurements. The dataset is divided into an 8:1:1 ratio for training, validation, and testing in Stage II multi-task learning process, as described in Sec. 4.3. This setup allows SoilNutri to be evaluated under real soil environments with natural variations in humidity, soil nutrient and texture.

As shown in Fig. 14 and Fig. 15, SoilNutri demonstrates stable prediction performance across different moisture and nitrogen ranges. For moisture estimation, both RMSE and MAE remain low overall, with average RMSE = 0.78% and MAE = 0.64%, and slightly higher errors observed at higher moisture levels (50–60% and > 60%). This increase reflects the stronger electromagnetic attenuation and scattering in wetter soils, which lower the signal-to-noise ratio and amplify reconstruction uncertainty. In contrast, mid-range moisture conditions (30–50%) maintain smaller errors for both metrics, indicating a favorable balance between signal penetration and soil-metasurface coupling.

For nitrogen prediction, the model achieves stable performance across low-to-medium concentrations (10–40 ppm) with a gradual increase in both RMSE and MAE at higher levels (> 50 ppm). On average, RMSE = 6.02 ppm and MAE = 5.14 ppm, demonstrating ppm-level precision. The observed increase at higher concentrations is attributed to temperature- and concentration-dependent ionic conductivity, where elevated nitrate ion levels enhance conductive losses and dielectric dispersion, thereby weakening reflected signal coherence. Overall, these results indicate that the system can capture agronomically meaningful variations across soil types, consistent with expected RF propagation and dielectric-response mechanisms in soil.

6.3 Impact of Deployment Depth on Sensing Accuracy

As shown in Fig. 16, the prediction accuracy of SoilNutri remains consistent across different deployment depths. For soil moisture estimation, the MAE slightly increases with depth, indicating that deeper underground placement (30–40 cm) introduces additional signal attenuation and multipath distortion due to longer propagation paths

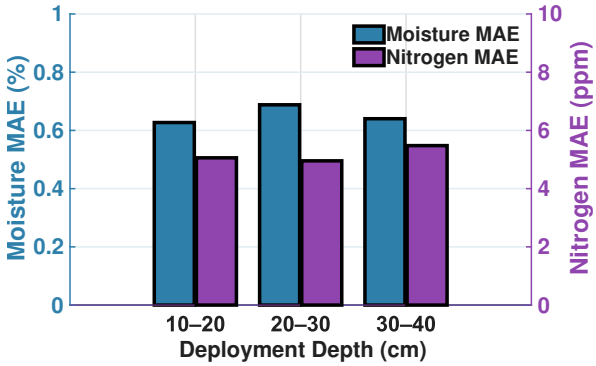

Fig. 16. Impact of deployment depth on sensing performance.

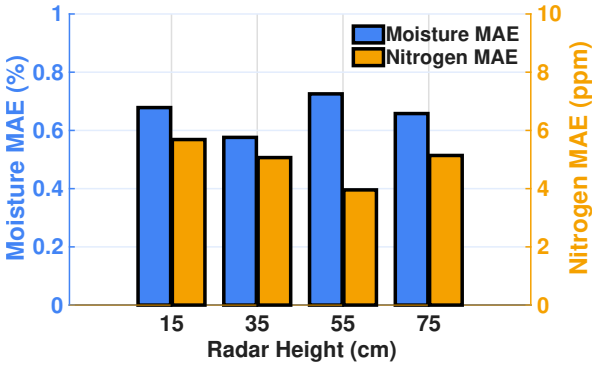

Fig. 17. Impact of radar height on sensing performance.

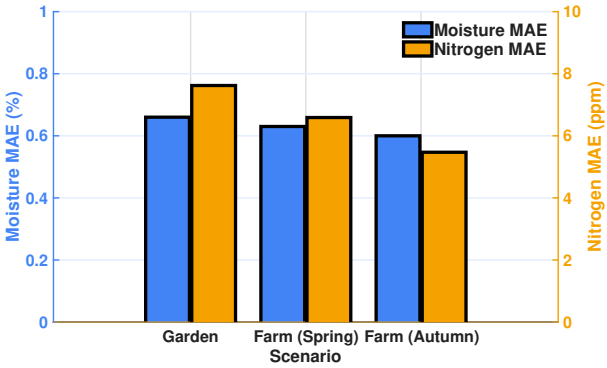

Fig. 18. Impact of seasonal and environmental scenarios.

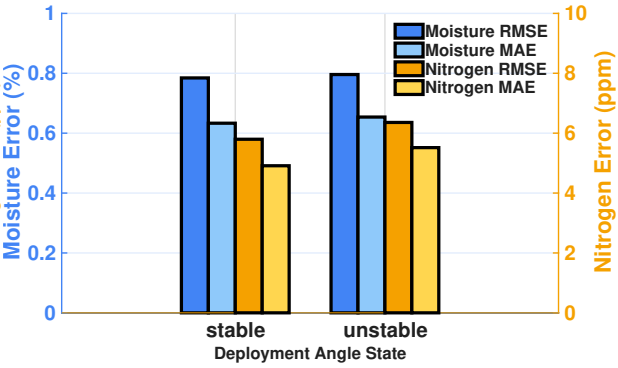

Fig. 19. Impact of different angles of radar holder.

through lossy media. However, the MAE across all depth groups remains within 1%, showing that the reconstructed reflection features preserve reliable amplitude–phase consistency even under stronger attenuation conditions.

For nitrogen prediction, a similar trend is observed: the MAE increases modestly as the metasurface capsule is deployed deeper into the soil. At shallow depths (10–20 cm), the reflected signals experience less dielectric loss, leading to lower MAE values, while deeper deployments (30–40 cm) suffer from higher conductive losses and reduced signal-to-noise ratio. This pattern is consistent with the frequency-dependent dielectric dispersion of moist soils, where both water and nitrate ions contribute to energy absorption at higher depths. Overall, the results indicate that SoilNutri maintains robust sensing performance across various soil burial depths, validating its suitability for in-field, non-invasive soil monitoring applications.

6.4 Impact of Radar Height on Sensing Accuracy

As shown in Fig. 17, radar height has a noticeable influence on the sensing accuracy of both moisture and nitrogen estimation. When the radar is positioned at a lower height (15 cm), the MAE values for both parameters increase due to stronger near-field interference and imperfect signal coupling between the radar and metasurface. This close proximity increases mutual coupling and multipath reflection at the soil–air interface, leading to elevated measurement noise.

At moderate radar heights (35 cm and 55 cm), SoilNutri achieves the lowest overall MAE, indicating that this range provides an optimal balance between signal strength and propagation stability. Here, the radar–metasurface alignment ensures sufficient signal-to-noise ratio while minimizing reflection distortion, resulting in more accurate feature reconstruction and regression.

As the radar height further increases to 75 cm, the sensing accuracy slightly decreases, particularly for nitrogen estimation. This degradation can be attributed to the increased free-space path loss and reduced backscattered signal amplitude, which weaken the spectral distinctiveness of the reflected waveform. Overall, the results confirm that SoilNutri maintains reliable performance across different radar heights, with the 35–55 cm range representing the most favorable configuration for field deployment.

6.5 Impact of Seasonal and Environmental Scenarios on Sensing Performance

In this section, we evaluate the cross-scenario and seasonal performance of SoilNutri across three representative environments: a small garden, farmland in spring before sowing, and the same farmland in autumn after crop growth, as summarized in Fig. 18. The seasonal comparison focuses on the farmland cases, where soybean cultivation and soil nutrient dynamics introduce natural variations in moisture and nitrogen levels. As shown in Fig. 18, SoilNutri maintains consistent sensing accuracy across these diverse environments, demonstrating its robustness under varying soil conditions and seasonal transitions.

For moisture estimation, the MAE remains stable within a narrow range from 0.66% to 0.60%, indicating that the reconstructed spectral features are largely unaffected by changes in soil surface texture or compactness across seasons. Nitrogen estimation, however, exhibits more noticeable variation. During the garden and early-spring farm measurements, the overall nitrogen concentration in the soil is relatively low, leading to weaker ionic polarization and smaller contrast in dielectric dispersion. These factors reduce the signal-to-noise ratio of the reflected spectrum and result in higher prediction errors, with MAE values of 7.62 ppm in the garden and 6.59 ppm in the spring farm scenario. In contrast, the autumn dataset corresponds to post-harvest conditions when the soil becomes more fertile and nitrogen concentration increases, thereby enhancing the electromagnetic response and improving the prediction accuracy to 5.47 ppm.

Overall, these results highlight that while the sensing performance of SoilNutri remains robust across heterogeneous soil environments, seasonal nutrient variations can subtly affect spectral discriminability. Nevertheless, the consolidated metasurface array and β-VAE reconstruction framework enable reliable ppm-level nitrogen estimation across diverse agricultural scenarios, confirming the system's adaptability to real-world field conditions.

6.6 Impact of Radar Holder Angle on Sensing Accuracy

As shown in Fig. 19, the deployment angle of the metasurface capsule exhibits a clear impact on the sensing accuracy for both soil moisture and nitrogen estimation. Here, the term *unstable* refers to scenarios where the upground radar platform is not perfectly level, typically involving a tilt angle within about 10° relative to the horizontal plane. For example, when the tripod is placed on uneven terrain or when the drone-mounted radar is affected by wind-induced tilting. Such angular misalignment introduces a non-perpendicular incidence between the radar beam and the metasurface plane, thereby altering the reflection geometry and reducing the effective coupling efficiency.

Quantitatively, the unstable configuration leads to higher prediction errors across both modalities. For moisture estimation, the RMSE and MAE increase from 0.78% and 0.64% under stable conditions to 0.82% and 0.68%, respectively. Similarly, for nitrogen prediction, the RMSE rises from 5.5 ppm to 5.9 ppm, and the MAE increases from 4.8 ppm to 5.3 ppm. These results indicate that even minor angular deviations can amplify spectral distortion and degrade the amplitude–phase coherence of the received signal, resulting in higher reconstruction and regression errors.

In contrast, the stable configuration maintains consistent radar–metasurface coupling and symmetric backscattering geometry, enabling more accurate spectral reconstruction and regression. Overall, this analysis highlights that maintaining horizontal stability of the radar platform—whether using a fixed tripod or an airborne carrier—is essential for ensuring accurate and repeatable soil parameter estimation in real-world deployments.

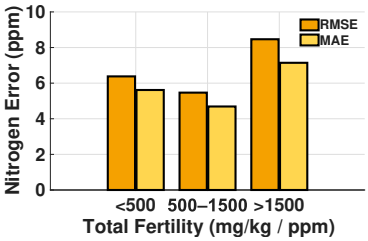

Fig. 20. Nitrogen sensing performance under different total fertility levels.

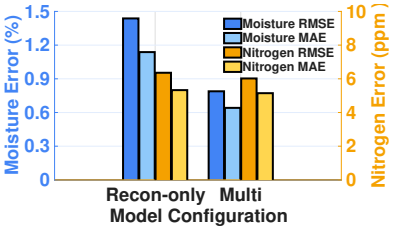

Fig. 21. Joint multi-task optimization: comparison between reconstruction-only and joint multi-task configurations.

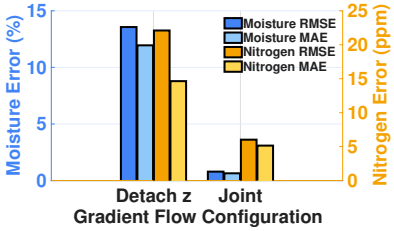

Fig. 22. Effect of gradient detachment (*Stop-Grad*) on the shared-latent representation.

Moreover, the consolidated metasurface array combined with β-VAE reconstruction framework inherently provides a certain degree of tolerance to angular variation. By jointly learning amplitude correlations and reconstructing distorted spectral features, the model effectively compensates for moderate changes in the incidence angle and polarization alignment. This property mitigates the degradation caused by minor tilts of the radar holder, allowing SoilNutri to maintain stable sensing performance under realistic field conditions where perfect horizontal alignment cannot always be guaranteed.

6.7 Impact of Total Fertility

In this section, we evaluate the impact of total soil fertility on nitrogen sensing performance. In natural soil environments, multiple macronutrients such as nitrogen, phosphorus, and potassium jointly contribute to the overall soil fertility and electrical conductivity. Although nitrogen is the primary indicator of crop growth, excessive or insufficient concentrations of other nutrients can alter the soil's dielectric behavior and thus interfere with nitrogen-specific spectral sensing.

To investigate this relationship, we categorize the soil samples into three fertility levels: below 500 mg/kg (raw soil with minimal fertilization), 500–1500 mg/kg (balanced fertilization with nitrogen-dominated composition), and above 1500 mg/kg (fertilizer-rich soil containing substantial additional nutrients). As shown in Fig. 20, the nitrogen prediction achieves the best performance in the medium-fertility range, where the MAE and RMSE reach approximately 6.5 ppm and 7.2 ppm, respectively. In contrast, low-fertility soils (<500 mg/kg) exhibit higher prediction errors due to weak ionic polarization and poor radar–metasurface coupling, while high-fertility soils (>1500 mg/kg) also cause error increases because the excessive concentration of other ions disturbs the nitrogen-related dielectric dispersion.

Overall, the results suggest that a moderate total fertility level (500–1500 mg/kg) provides the most favorable electromagnetic response for nitrogen sensing, balancing ion-induced signal strength and compositional selectivity. This observation highlights the practical importance of maintaining balanced soil nutrient composition for achieving reliable in-field nitrogen estimation.

6.8 Ablation Study

To further understand the contribution of each design component in SoilNutri, we perform a series of ablation studies focusing on two key aspects: (*i*) the role of joint multi-task learning in improving latent representation quality, and (*ii*) the impact of gradient flow from the prediction heads on the shared latent space.

Impact of Joint Multi-task Optimization. While the reconstruction branch ensures spectral fidelity by restoring the intrinsic reflection patterns of the metasurface, the prediction heads are designed to infer soil moisture and nitrogen concentrations from the reconstructed latent space. By comparing the reconstruction-only baseline with

the joint multi-task configuration, we assess how integrating reconstruction and prediction objectives enhances spectral discriminability and environmental robustness. As shown in Fig. 21, both moisture and nitrogen estimation benefit from the joint multi-task design after rescaling the metrics to comparable ranges. For moisture, the RMSE and MAE are reduced by approximately 45%, confirming the improvement in spectral reconstruction and latent feature consistency. Nitrogen prediction also shows stable improvement, demonstrating that the shared β-VAE latent space effectively transfers spectral information between reconstruction and regression tasks.

Effect of Gradient Feedback to the Latent Space. To further examine the contribution of prediction supervision, we introduce a *stop-gradient* setting that detaches the gradient flow from the prediction heads to the shared latent space. As shown in Fig. 22, blocking the gradient feedback results in a dramatic degradation in both moisture and nitrogen prediction accuracy. Specifically, the moisture MAE increases from 0.64% to 11.95%, and the nitrogen MAE rises from 5.15 ppm to 14.64 ppm, confirming that gradient feedback from the prediction objectives is essential for shaping a task-discriminative latent representation. In contrast, the full-gradient joint training configuration maintains low RMSE and MAE across both modalities, highlighting that predictive supervision helps align the shared β-VAE latent space with task-relevant spectral variations.

7 DISCUSSION

Extending Sensing Depth for Soil Sensing. The current SoilNutri prototype employs a UWB radar centered around 7 GHz. This design prioritizes spectral resolution for metasurface-based sensing but inherently limits penetration depth due to higher soil attenuation at elevated frequencies. A natural extension is to explore lower-frequency UWB bands in the 1–3 GHz range, which can improve soil penetration while retaining sufficient bandwidth to resolve metasurface-induced resonance features, enabling deeper root-zone sensing and layered soil profiling. Beyond UWB, lower-frequency RF modalities such as LoRa and WiFi may further extend sensing depth but face fundamental bandwidth constraints that challenge conventional resonance-based metasurface designs. Addressing this trade-off motivates future research that jointly considers RF modality selection, metasurface structure, and learning-based inference to extend sensing depth without sacrificing sensing fidelity.

Improving Robustness to Temperature Variations in Soil Sensing. Temperature variations can affect soil moisture and nitrogen sensing by altering the dielectric properties of soil and water, including the temperature-dependent permittivity of water and nitrate detection. In this study, all experiments were conducted under relatively stable ambient temperatures of approximately 15 °C, representative of typical spring and autumn field conditions. As a future direction, incorporating temperature-aware modeling, such as learning temperature-dependent calibration factors or integrating auxiliary temperature measurements into the inference pipeline, could further improve sensing robustness under diverse environmental conditions.

Tripod vs UAV Deployment Trade-offs for Field Data Collection. Tripod-based deployment provides a highly stable sensing geometry by eliminating motion-induced spectral distortion, but its practicality in large farmland settings is limited by uneven terrain and the labor required for manual relocation. In contrast, UAV-assisted deployment improves mobility and spatial coverage by enabling measurements at discrete hovering locations above buried metasurface capsules, reducing dependence on ground conditions. However, UAV-based measurements are more sensitive to environmental factors such as wind-induced tilting and standoff variation, which can affect signal quality. As a result, UAV-assisted sensing is better suited for calm conditions and large-area surveys, while tripod-based deployment remains preferable when maximum measurement stability is required.

Toward Mobile and Commodity UWB Platforms for Soil Sensing. Recent smartphones increasingly integrate UWB radios operating in the 6-8 GHz band, reflecting the growing availability of compact and mobile UWB hardware beyond specialized sensing platforms. If controlled access to low-level UWB measurements becomes available in the future, the passive and battery-free design of SoilNutri naturally aligns with such

commodity devices, as sensing is fully offloaded to buried metasurfaces without requiring powered underground components. This capability enables integration with mobile carriers such as handheld devices or UAVs, supporting scalable, on-demand soil sensing with minimal infrastructure and highlighting the sustainability of long-term, maintenance-free deployment.

Preserving Soil Fertility in Situ. SoilNutri focuses on in situ monitoring of soil fertility to prevent excessive fertilization while maintaining essential nutrient levels for precision agriculture applications. However, the current system does not provide active interventions to mitigate nutrient leaching, soil acidification, or long-term soil degradation. To further preserve soil fertility in situ, we plan to integrate an advanced cementitious composite that has ultra-ductility and self-healing capability [4, 21, 26] to construct a durable interface that limits nutrient loss. This material offers high resistance to cracking and selective permeability that blocks the transport of soil nutrients from farmland into surrounding areas, while still allowing water infiltration.

8 RELATED WORK

In this section, we review prior studies most relevant to SoilNutri. For clarity, we categorize these systems into two groups: RF signal-based soil sensing and tag-assisted soil sensing approaches.

RF Signal-based Soil Sensing. A number of prior works utilize radio frequency (RF) signals—such as Wi-Fi, LoRa, LTE, and UWB—to enable soil moisture sensing. Strobe [14] employs commodity Wi-Fi devices to achieve centimeter-level depth sensing, though its effective range remains limited. Chang et al. [10] harness the long-range transmission and through-wall penetration of LoRa to enable soil sensing at greater depths. LTE-Soil-Meter[16] demonstrates a sensing coverage of up to 2.4 km using LTE infrastructure. Ultra-wideband (UWB)-based systems such as SoilID [15] and the work by Josephson et al. [22] provide deeper subsurface penetration (up to 30–38 cm), although they rely on custom hardware, which may increase system cost. More recently, MetaSoil [12] explores the use of mmWave signals for soil moisture sensing, achieving promising depth performance with moderate deployment cost and low measurement error.

Tag-based Soil Sensing. Tag-based approaches incorporate physical tags as sensing elements for soil monitoring. GreenTag [43] employs passive RFID tags affixed to planting pots, offering an ultra-low-cost solution with limited sensing range. SoilTag [20] utilizes Wi-Fi backscatter to achieve a longer sensing distance of up to 13.9 m with minimal power consumption. CoMEt [24] leverages high-end USRP X310 radios to reach sensing depths of 38 cm, albeit at the cost of expensive hardware. SoilCare [44] combines LoRa with VNIR spectroscopy to monitor both soil moisture and nutrient content but requires a sealed box for underground deployment.

In contrast to these prior methods that predominantly focus on moisture sensing, SoilNutri enables simultaneous monitoring of both soil moisture and nitrogen concentration. It reliably distinguishes between different types of soil constituents, offering high-resolution, multi-parameter sensing in a compact, battery-free form factor.

9 CONCLUSION

This work presents SoilNutri, a low-cost, battery-free metasurface sensing system for the joint monitoring of soil moisture and nitrogen. By integrating a complementary split-ring CSR metasurface within a sandwich-structured capsule, SoilNutri achieves stable underground operation with high sensitivity to both moisture and nitrogen content. A lightweight soil-meta-VAE framework leverages a unified latent space to restore soil-distorted reflection spectra and enable simultaneous estimation of soil moisture and nitrogen concentration. Extensive in-lab and field evaluations demonstrate high-precision moisture estimation with 0.64% MAE and ppm-level nitrogen prediction with 5.14 ppm MAE across diverse soil types, depths, and seasonal conditions. With a per-unit cost below $1 and a reusable encapsulated design, SoilNutri provides a scalable, sustainable, and physically interpretable solution for multi-nutrient, in-situ soil monitoring in next-generation smart agriculture.

References

[1] 2025. CST Studio Suite. https://www.3ds.com/products/simulia/cst-studio-suite

[2] Francisco Albornoz. 2016. Crop responses to nitrogen overfertilization: A review. *Scientia horticulturae* 205 (2016), 79–83.

[3] Leland C Allen. 1974. Physical Chemistry of Water: Water. A Comprehensive Treatise. Felix Franks, Ed. Plenum, New York, 1973. Vol. 1, The Physics and Physical Chemistry of Water. xx, 596 pp., illus. Vol. 2, Water in Crystalline Hydrates; Aqueous Solutions of Simple Nonelectrolytes. xx, 684 pp., illus. Vol. 3, Aqueous Solutions of Simple Electrolytes. xviii, 472 pp., illus. Each volume, 37.50;bysubscription, 32.50. *Science* 184, 4133 (1974), 152–152.

[4] Diego Aparicio, Matias Leon-Miquel, Junyi Duan, Juan Silva-Retamal, Qian Zhang, Chengcheng Tao, Qingxu Jin, and Alvaro Paul. 2025. Seismic and wind resistance of natural pozzolan-based engineered cementitious composites: material characterization and numerical analysis. *Materials and Structures* 58, 6 (2025), 227.

[5] Hossein Azadi, Saghi Movahhed Moghaddam, Stefan Burkart, Hossein Mahmoudi, Steven Van Passel, Alishir Kurban, and David Lopez-Carr. 2021. Rethinking resilient agriculture: From climate-smart agriculture to vulnerable-smart agriculture. *Journal of Cleaner Production* 319 (2021), 128602.

[6] Juan Domingo Baena, Jordi Bonache, Ferran Martín, R Marqués Sillero, Francisco Falcone, Txema Lopetegi, Miguel AG Laso, Joan Garcia-Garcia, Ignacio Gil, M Flores Portillo, et al. 2005. Equivalent-circuit models for split-ring resonators and complementary split-ring resonators coupled to planar transmission lines. *IEEE transactions on microwave theory and techniques* 53, 4 (2005), 1451–1461.

[7] Norman Born, Marco Reuter, Martin Koch, and Maik Scheller. 2013. High-Q terahertz bandpass filters based on coherently interfering metasurface reflections. *Optics letters* 38, 6 (2013), 908–910.

[8] Christophe Caloz and Tatsuo Itoh. 2005. *Electromagnetic metamaterials: transmission line theory and microwave applications*. John Wiley & Sons.

[9] Liqiong Chang, Xiaofeng Yang, Ruyue Liu, Guodong Xie, Fuwei Wang, and Ju Wang. 2024. FSS-Tag: High Accuracy Material Identification System Based On Frequency Selective Surface Tag. *Proceedings of the ACM on Interactive, Mobile, Wearable and Ubiquitous Technologies* 7, 4 (2024), 1–24.

[10] Zhaoxin Chang, Fusang Zhang, Jie Xiong, Junqi Ma, Beihong Jin, and Daqing Zhang. 2022. Sensor-free soil moisture sensing using lora signals. *Proceedings of the ACM on Interactive, Mobile, Wearable and Ubiquitous Technologies* 6, 2 (2022), 1–27.

[11] Baicheng Chen, John Nolan, and Xinyu Zhang. 2024. MetaBioLiq: A Wearable Passive Metasurface Aided mmWave Sensing Platform for BioFluids. In *Proceedings of the 30th Annual International Conference on Mobile Computing and Networking*. 1192–1206.

[12] Baicheng Chen, John Nolan, Xinyu Zhang, and Wan Du. 2024. MetaSoil: Passive mmWave Metamaterial Multi-layer Soil Moisture Sensing. In *Proceedings of the 22nd ACM Conference on Embedded Networked Sensor Systems*. 225–238.

[13] Mohammad Cheraghinia, Adnan Shahid, Stijn Luchie, Gert-Jan Gordebeke, Olivier Caytan, Jaron Fontaine, Ben Van Herbruggen, Sam Lemey, and Eli De Poorter. 2024. A comprehensive overview on uwb radar: Applications, standards, signal processing techniques, datasets, radio chips, trends and future research directions. *IEEE Communications Surveys & Tutorials* (2024).

[14] Jian Ding and Ranveer Chandra. 2019. Towards low cost soil sensing using Wi-Fi. In *The 25th annual international conference on mobile computing and networking*. 1–16.

[15] Rong Ding, Haiming Jin, Dong Xiang, Xiaocheng Wang, Yongkui Zhang, Dingman Shen, Lu Su, Wentian Hao, Mingyuan Tao, Xinbing Wang, et al. 2023. Soil moisture sensing with uav-mounted ir-uwb radar and deep learning. *Proceedings of the ACM on Interactive, Mobile, Wearable and Ubiquitous Technologies* 7, 1 (2023), 1–25.

[16] Yuda Feng, Yaxiong Xie, Deepak Ganesan, and Jie Xiong. 2022. Lte-based low-cost and low-power soil moisture sensing. In *Proceedings of the 20th ACM Conference on Embedded Networked Sensor Systems*. 421–434.

[17] Ian Goodfellow, Jean Pouget-Abadie, Mehdi Mirza, Bing Xu, David Warde-Farley, Sherjil Ozair, Aaron Courville, and Yoshua Bengio. 2020. Generative adversarial networks. *Commun. ACM* 63, 11 (2020), 139–144.

[18] Kaiming He, Xinlei Chen, Saining Xie, Yanghao Li, Piotr Dollár, and Ross Girshick. 2022. Masked autoencoders are scalable vision learners. In *Proceedings of the IEEE/CVF conference on computer vision and pattern recognition*. 16000–16009.

[19] Jonathan Ho, Ajay Jain, and Pieter Abbeel. 2020. Denoising diffusion probabilistic models. *Advances in neural information processing systems* 33 (2020), 6840–6851.

[20] Wenli Jiao, Ju Wang, Yelu He, Xiangdong Xi, and Fuwei Wang. 2023. SoilTAG: fine-grained soil moisture sensing through chipless tags. *IEEE Transactions on Mobile Computing* 23, 3 (2023), 2153–2170.

[21] Qingxu Jin and Victor C Li. 2019. Structural and durability assessment of ECC/concrete dual-layer system for tall wind turbine towers. *Engineering Structures* 196 (2019), 109338.

[22] Colleen Josephson, Manikanta Kotaru, Keith Winstein, Sachin Katti, and Ranveer Chandra. 2021. Low-cost in-ground soil moisture sensing with radar backscatter tags. In *Proceedings of the 4th ACM SIGCAS Conference on Computing and Sustainable Societies*. 299–311.

[23] Darko Kajfez and Eugene J Hwan. 1984. Q-factor measurement with network analyzer. *IEEE transactions on microwave theory and techniques* 32, 7 (1984), 666–670.

[24] Usman Mahmood Khan and Muhammad Shahzad. 2022. Estimating soil moisture using RF signals. In *Proceedings of the 28th annual international conference on mobile computing and networking*. 242–254.

[25] Apoorva Kulkarni and Ramani Narayan. 2023. Morphology, mechanical properties, and biodegradability of modified thermoplastic starch/PETG blends with in situ generated graft copolymers. *Sustainability* 15, 3 (2023), 2227.

[26] Matias Leon-Miquel, Juan Silva-Retamal, Diego Aparicio, Milena Rangelov, Qingxu Jin, and Alvaro Paul. 2023. Novel application of Chilean natural pozzolan for sustainable strain-hardening cementitious composite. *Resources, Conservation and Recycling* 197 (2023), 107098.

[27] Leslie Lipper, Philip Thornton, Bruce M Campbell, Tobias Baedeker, Ademola Braimoh, Martin Bwalya, Patrick Caron, Andrea Cattaneo, Dennis Garrity, Kevin Henry, et al. 2014. Climate-smart agriculture for food security. *Nature climate change* 4, 12 (2014), 1068–1072.

[28] Yimeng Liu, Maolin Gan, Gen Li, Younsuk Dong, and Zhichao Cao. 2025. Adonis: Neural-enhanced Fine-grained Leaf Wetness Sensing with Efficient mmWave Imaging. In *Proceedings of IEEE INFOCOM*.

[29] Yimeng Liu, Maolin Gan, Huaili Zeng, Li Liu, Younsuk Dong, and Zhichao Cao. 2024. Hydra: Accurate multi-modal leaf wetness sensing with mm-wave and camera fusion. In *Proceedings of the 30th Annual International Conference on Mobile Computing and Networking*. 800–814.

[30] Yimeng Liu, Maolin Gan, Huaili Zeng, Yidong Ren, Gen Li, Younsuk Dong, Xiaobo Tan, and Zhichao Cao. 2025. Proteus: : Enhanced mmWave Leaf Wetness Detection with Cross-Modality Knowledge Transfer. In *Proceedings of ACM SenSys*.

[31] Junqi Ma, Fusang Zhang, Beihong Jin, Chang Su, Siheng Li, Zhi Wang, and Jiazhi Ni. 2024. Push the limit of highly accurate ranging on commercial uwb devices. *Proceedings of the ACM on Interactive, Mobile, Wearable and Ubiquitous Technologies* 8, 2 (2024), 1–27.

[32] Ricardo Marqués, Francisco Mesa, Jesus Martel, and Francisco Medina. 2003. Comparative analysis of edge-and broadside-coupled split ring resonators for metamaterial design-theory and experiments. *IEEE Transactions on antennas and propagation* 51, 10 (2003), 2572–2581.

[33] David Molden. 2013. *Water for food water for life: A comprehensive assessment of water management in agriculture*. Routledge.

[34] Alexander Quinn Nichol and Prafulla Dhariwal. 2021. Improved denoising diffusion probabilistic models. In *International conference on machine learning*. PMLR, 8162–8171.

[35] NOVELDA. 2025. NOVELDA Ultra-wideband Impulse Radar Transceiver SoC. https://novelda.com/technology/datasheets/

[36] Keiron O'shea and Ryan Nash. 2015. An introduction to convolutional neural networks. *arXiv preprint arXiv:1511.08458* (2015).

[37] Soil Quality. 2025. Soil Nitrogen Supply. https://www.soilquality.org.au/factsheets/soil-nitrogen-supply

[38] Yidong Ren, Wei Sun, Jialuo Du, Huaili Zeng, Younsuk Dong, Mi Zhang, Shigang Chen, Yunhao Liu, Tianxing Li, and Zhichao Cao. 2024. Demeter: Reliable cross-soil lpwan with low-cost signal polarization alignment. In *Proceedings of the 30th Annual International Conference on Mobile Computing and Networking*. 230–245.

[39] Ivan W Selesnick. 2011. Wavelet transform with tunable Q-factor. *IEEE transactions on signal processing* 59, 8 (2011), 3560–3575.

[40] Alberto Solera-Rico, Carlos Sanmiguel Vila, Miguel Gómez-López, Yuning Wang, Abdulrahman Almashjary, Scott TM Dawson, and Ricardo Vinuesa. 2024. β-variational autoencoders and transformers for reduced-order modelling of fluid flows. *Nature Communications* 15, 1 (2024), 1361.

[41] Xue Sun, Jie Xiong, Chao Feng, Xiaohui Li, Jiayi Zhang, Binghao Li, Dingyi Fang, and Xiaojiang Chen. 2024. Gastag: A gas sensing paradigm using graphene-based tags. In *Proceedings of the 30th Annual International Conference on Mobile Computing and Networking*. 342–356.

[42] Odysseas Tsilipakos, Thomas Koschny, and Costas M Soukoulis. 2018. Antimatched electromagnetic metasurfaces for broadband arbitrary phase manipulation in reflection. *ACS photonics* 5, 3 (2018), 1101–1107.

[43] Ju Wang, Liqiong Chang, Shourya Aggarwal, Omid Abari, and Srinivasan Keshav. 2020. Soil moisture sensing with commodity RFID systems. In *Proceedings of the 18th International Conference on Mobile Systems, Applications, and Services*. 273–285.

[44] Juexing Wang, Yuda Feng, Gouree Kumbhar, Guangjing Wang, Qiben Yan, Qingxu Jin, Robert C Ferrier, Jie Xiong, and Tianxing Li. 2024. SoilCares: Towards low-cost soil macronutrient and moisture monitoring using RF-VNIR sensing. In *Proceedings of the 22nd Annual International Conference on Mobile Systems, Applications and Services*. 196–209.

[45] Amir H Wolfe and Jonathan A Patz. 2002. Reactive nitrogen and human health: acute and long-term implications. *Ambio: A journal of the human environment* 31, 2 (2002), 120–125.

[46] Binbin Xie, Deepak Ganesan, and Jie Xiong. 2022. Embracing lora sensing with device mobility. In *Proceedings of the 20th ACM Conference on Embedded Networked Sensor Systems*. 349–361.

[47] Yong Yang, Ying Chen, Xiaolan Zhang, Edwin Ongley, and Lei Zhao. 2012. Methodology for agricultural and rural NPS pollution in a typical county of the North China Plain. *Environmental Pollution* 168 (2012), 170–176.

[48] Fusang Zhang, Jie Xiong, Zhaoxin Chang, Junqi Ma, and Daqing Zhang. 2022. Mobi2Sense: empowering wireless sensing with mobility. In *Proceedings of the 28th Annual International Conference on Mobile Computing And Networking*. 268–281.

[49] Hanqiao Zhang, Steven Krooswyk, and Jeffrey Ou. 2015. *High speed digital design: design of high speed interconnects and signaling*. Elsevier.